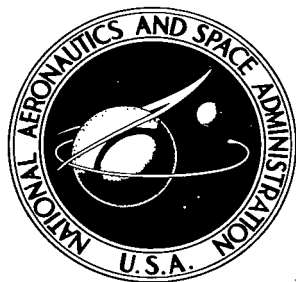


NASA TECHNICAL NOTE



NASA TN D-3269

c. 1

LOAN COPY: REI
AFWL (WLI)
KIRTLAND AFB,

0079832



TECH LIBRARY KAFB, NM

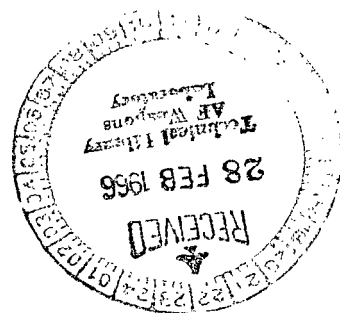
NASA TN D-3269

AN INVESTIGATION OF HIGHLY UNDEREXPANDED EXHAUST PLUMES IMPINGING UPON A PERPENDICULAR FLAT SURFACE

by Allen R. Vick and Earl H. Andrews, Jr.

Langley Research Center

Langley Station, Hampton, Va.



TECH LIBRARY KAFB, NM



0079832

NASA TN D-3269

AN INVESTIGATION OF HIGHLY UNDEREXPANDED EXHAUST PLUMES
IMPINGING UPON A PERPENDICULAR FLAT SURFACE

By Allen R. Vick and Earl H. Andrews, Jr.

Langley Research Center
Langley Station, Hampton, Va.

NATIONAL AERONAUTICS AND SPACE ADMINISTRATION

For sale by the Clearinghouse for Federal Scientific and Technical Information
Springfield, Virginia 22151 - Price \$3.00

AN INVESTIGATION OF HIGHLY UNDEREXPANDED EXHAUST PLUMES
IMPINGING UPON A PERPENDICULAR FLAT SURFACE

By Allen R. Vick and Earl H. Andrews, Jr.
Langley Research Center

SUMMARY

An investigation has been conducted to determine the effects of highly underexpanded nozzle exhaust plumes impinging upon a flat surface mounted perpendicular to the nozzle axis. Impingement-surface static-pressure data were obtained in an experimental program conducted in the Langley 41-foot-diameter vacuum sphere. Unheated air having a pressure of approximately 2400 psia (16.55×10^6 N/m²) was exhausted from two different nozzles; a converging nozzle having an exit Mach number of 1.0, and a converging-diverging nozzle with a nominal design exit Mach number of 5.0. Data were obtained continuously for ratios of nozzle total pressure to ambient pressure ranging from approximately 250×10^3 down to 50×10^3 for various separation distances of the nozzle exit from the impingement surface. Also included is a comparison of the experimental data with some theoretically calculated results.

The results of this investigation showed three different shock structures within the exhaust plume which were dependent upon the distances from the nozzle exit to the impingement surface and the ratio of the nozzle total pressure to the ambient pressure. The three types of shock structures consisted of (1) a surface shock located at a constant distance from the surface, (2) a shock acting similar to a Mach disk, which was located closer to the nozzle exit than it would be if no impingement surface were present and for which the distance from the nozzle exit decreased as the ratio of nozzle total pressure to ambient pressure decreased, and (3) a crossed oblique shock with a near-normal shock adjacent to the impingement surface. The type of shock exerted considerable influence on the surface-pressure distributions. At small distances from the nozzle exit to the surface and with the surface shock at a constant standoff distance, maximum surface pressures occurred on the nozzle axis and decreased in a smooth continuous manner with increasing radial distances. For these conditions a single curve was found to represent the radial variation of the ratio of the surface static pressure to the nozzle total pressure for the entire range of test pressure ratios. As the distance from the nozzle exit to the surface increased, maximum surface pressures occurred around an annulus followed by an irregular radial variation in surface pressure. The crossed oblique shock formation was accompanied by an instantaneous increase in surface pressures. Comparisons of theoretical and experimental axial center-line Mach numbers and impingement-surface pressures were in fair agreement.

INTRODUCTION

Nozzles operating in near-vacuum environments produce exhaust gases which expand to extremely large sizes following expulsion from the nozzle. When any part of the main vehicle or other adjacent structure becomes either partly or totally submerged in these plumes, various problems may arise. Many of the problems associated with these highly expanded exhaust plumes are summarized in reference 1 and include such items as: (1) exhaust backflow from clusters of nozzles in which the interference between adjacent plumes causes a reverse flow of hot exhaust gases, which in turn imposes a convective heat load on the exposed vehicle components, (2) the attenuation of electromagnetic signals, which usually occurs when the exhaust plume becomes large enough to intercept the line of sight between the vehicle antenna and the ground-tracking stations, (3) aerodynamic stability and control which can be affected if the jet plume produces extensive boundary-layer separation so that control surfaces located in the affected area will be subject to loss in effectiveness, and (4) plume interactions with adjacent surfaces. The latter item is of particular concern since direct plume impingement results in pressure forces on the affected surfaces, and such pressure forces are usually adverse. During rocket-stage separation, for example, upper-stage ignition too soon after stage separation produces interference pressure forces on the upper stage which can adversely affect the performance of the upper stage (ref. 2).

An additional problem area for which no published information exists concerns exhaust-gas interference during docking maneuvers between orbiting spacecraft where the exhaust gases from one maneuvering vehicle impinge upon the other. The impingement of high velocity gases on the passive member of two docking vehicles will produce forces which will adversely affect the neutral stability of that vehicle and could necessitate costly fuel expenditures for corrective measures.

The many unknowns of space flight also include hazards arising during either landing or take-off from the lunar surface. These hazards depend to some extent on the position of the vehicle above the impingement surface and include such items as surface erosion and the subsequent formation of craters, possible damage to surrounding lunar bases as a result of flying debris, dust-cloud interference with visibility and navigation, and the reflection of hot gases back onto the vehicle. These problem areas are intensified somewhat by the uncertainty as to the exact composition of the lunar surface; this uncertainty requires that all possibilities be explored fully to insure maximum safety to spacecraft and personnel. Although a few investigations have been made already, both theoretically (refs. 3 to 5) and experimentally (refs. 6 to 11), much remains to be investigated and learned. The present investigation was initiated to supplement the knowledge obtained from previous investigations. The purpose of the present investigation was to determine

experimentally over a wide range of nozzle-pressure ratios the exhaust-plume impingement pressures on a flat surface located at various positions normal to the plume axis and to compare some of these results with those determined theoretically.

The investigation reported herein was conducted in the Langley 41-foot-diameter vacuum sphere for ratios of nozzle total pressure to ambient pressure varying from about 250×10^3 down to 50×10^3 . Two test nozzles with exit Mach numbers of 1.0 and 5.0 (inviscid design) exhausted air at a total temperature and pressure of approximately 90° F (305° K) and 2400 psia ($16.55 \times 10^6 \text{ N/m}^2$), respectively, onto a flat surface normal to the nozzle axis. The location of the impingement surface relative to the nozzle exit was varied over a range of positions for both nozzles. Data were obtained in the form of impingement-surface static-pressure measurements and high-speed schlieren motion pictures.

SYMBOLS

The units used for physical quantities in this paper are given both in the U.S. Customary Units and in the International System of Units (SI). Factors relating the two systems are given in reference 12 and those used in the present investigation are presented in the appendix.

d	diameter
d_{th}	throat diameter
l	distance along nozzle axis from nozzle exit to location of exhaust-jet Mach disk
M	Mach number
p	pressure
r	radial distance from nozzle axis
x	distance downstream of nozzle exit
γ	ratio of specific heats
θ_n	nozzle expansion half-angle
ψ	angle, used in defining location of pressure orifices, on flat plate, measured clockwise when viewing plate from upstream side (see fig. 2)

Subscripts:

exp	experimental
j	nozzle exit
max	maximum
min	minimum
s	impingement surface
t	total
1	conditions just upstream of a shock
2	conditions just downstream of a shock
∞	ambient (in 41-foot (12.5 m) sphere)

APPARATUS AND PROCEDURE

Test Setup and Procedure

The experimental investigation was conducted in the Langley 41-foot-diameter vacuum sphere with the test setup shown in figure 1(a). The unheated air, dried to a dew-point of about -40° F (233° K), had a total temperature and pressure of approximately 90° F (305° K) and 2400 psia (16.55×10^6 N/m²), respectively, and the available air volume was sufficient to maintain an essentially constant nozzle stagnation pressure during a test. An enlargement of the test setup, shown in the insert of figure 1(a), shows the general arrangement of the nozzle, impingement surface, and schlieren mirror.

The impingement surface, a flat rectangular plate, was mounted perpendicular to the nozzle axis. Surface pressures were measured with the plate located 20, 40, 80, 160, 240, and 400 nozzle exit diameters downstream of the exit of a Mach 1.0 nozzle and 4, 8, 20, 40, and 80 nozzle-exit diameters downstream of the exit of a nominal Mach 5.0 nozzle. The center point of the impingement surface was aligned with the nozzle axis.

Vacuum pumps were utilized to attain initial pretest pressures in the sphere of approximately 0.4 torr (0.0077 psia or 53.3 N/m²). During a total test time of approximately 15 seconds the ratio of the nozzle total pressure to ambient pressure was reduced from about 250×10^3 to 50×10^3 . With the test nozzle in operation, the vacuum-sphere pressure increased linearly with time; therefore, the ratio of total pressure to ambient pressure decreased hyperbolically with time.

Test Nozzles

The investigation was conducted with two nozzles, one convergent and the other convergent-divergent, as shown in figure 1(b). The converging nozzle ($M_j = 1.0$) had an exit diameter of 0.125 inch (0.318 cm) and the converging-diverging conical nozzle ($M_j = 5.0$ based on inviscid flow) had an exit diameter of 0.625 inch (1.588 cm), an expansion-area ratio of 25, and a half-angle of 15° . Previous investigations (refs. 13 and 14), using the same nozzles, showed, by use of a static-pressure orifice installed in the expansion wall near the exit, that for viscous flow the design nozzle of $M_j = 5.0$ actually had an indicated exit Mach number of 4.79. Unless otherwise indicated, the nozzle inviscid-design value of $M_j = 5.0$ is used throughout this paper.

Instrumentation

Nozzle stagnation pressure was measured by a 3000-psia (20.7×10^6 N/m²) pressure transducer located between the remotely operated solenoid valve and the nozzle inlet bell (as shown in insert of fig. 1(a)). The sphere ambient pressure was measured in the vicinity of the nozzle by a small differential pressure transducer with a range of 0.005 to 0.100 psia (34.5 to 689.5 N/m²). The impingement plate was instrumented with static-pressure orifices 0.040 inch (0.10 cm) in diameter located as shown in the polar coordinate sketch of figure 2; in some instances as many as six static-pressure orifices were located at a constant radius from the impingement-surface center point. All static-pressure orifices were connected to differential pressure transducers (NACA miniature-type inductive gage) by means of 9-inch (23-cm) lengths of plastic tubing to reduce possible vibrational effects and yet retain a rapid response time (about 40 milliseconds). Inasmuch as many of the gages were operating in the lower 20 percent of the range, the overall accuracy of the data is probably not so good as the rated accuracy of ± 0.5 percent. All pressure measurements were continuously recorded on oscillographs for the duration of each 15-second test.

High-speed double-pass schlieren movies (16 millimeter) were obtained for each test. Enlargements of individual frames were of poor quality and, therefore, deemed to be undesirable for reproduction. However, the schlieren movies proved to be very helpful in analyzing the data of this investigation.

Impingement Surface

The impingement surface was a rectangular plate with dimensions of 36 inches (91 cm) by 42 inches (107 cm). One quadrant of the plate is shown outlined in figure 2 with the pressure orifices located along radial lines originating at the center point of the plate. The radial lines are identified by the value of the angle ψ , measured in a clockwise direction when viewing the plate from the upstream side. Pressure instrumentation

was limited to only the quadrant shown except for the several orifices located within a 2-inch (5-cm) radius of the plate center point. In some instances as many as six static-pressure orifices are located at a constant radius.

RESULTS AND DISCUSSION

Jet Boundaries

In order to show the size and shape of the exhaust plumes relative to the impingement-surface location, theoretical plume boundaries were calculated by the method of characteristics for quiescent air without a plate in the plume with the use of three-dimensional irrotational equations of flow and the computer program described in reference 14. The results of these calculations are presented in figure 3 for each of the five ratios of nozzle total pressure to ambient pressure presented in the tables. The boundary coordinates are presented in nondimensional form as r/d_j and x/d_j . For purposes of illustration, the downstream locations of the impingement surface in terms of nozzle-exit diameter are superimposed on the figure for each of the various test separation distances. At impingement-surface locations (indicated by Roman numerals I to VI) beyond position III in figure 3(a), the plume size is larger than the 36- by 42-inch (91- by 107-cm) plate at some of the higher pressure ratios.

The related experiments of references 13 and 14, conducted with the nozzles used in this investigation, showed excellent agreement of the experimental boundaries with those calculated theoretically. However, as stated previously in "Apparatus and Procedure," the exit characteristics for the Mach 5.0 nozzle differed considerably from the inviscid-design values of $M_j = 5.0$ and $\theta_n = 15^\circ$. References 13 and 14 found the effective exit Mach number M_j to be 4.79 and the effective nozzle half-angle θ_n to be 26.5° as determined from measurements of the initial turning angle of the exhaust flow. The jet-plume boundaries for these effective exit characteristics are shown in figure 3(b).

Observed Characteristics of Shock Structures

The general quality of the schlieren movies was such that single-frame enlargements were not suitable for reproduction. Shock formations within the plumes and adjacent to the impingement surface however were readily evident in viewing the movies; observations of these movies proved to be of considerable value in analyzing the data. For example, three basic types of shock structures were found to exist (fig. 4), and are dependent upon the separation distance from the nozzle exit to the surface and the pressure ratio. The most frequently observed shock system (type I) consists of a surface shock located at a near-constant standoff distance from the impingement surface. This condition exists for either the very large pressure ratios experienced in near-vacuum operation, where the plume size is extremely large, or for small separation distances

from the nozzle to the surface such as those shown for positions I and II for both nozzles in figure 3. The second type of shock system, in which the surface shock ceases to remain at a constant standoff distance, is experienced as the pressure ratio p_t/p_∞ is varied for the surface positioned at greater downstream distances (positions III to VI for the $M_j = 1.0$ nozzle and III to V for the $M_j = 5.0$ nozzle). For these conditions (type II shock) the shock appears to act similar to a plume internal Mach disk which moves toward the nozzle exit as the pressure ratio is decreased. The third shock system (type III) is one in which two different types of shocks are present within the exhaust plume and occurs primarily during low-pressure-ratio operation. Basically, it consists of crossed oblique shocks followed by a normal shock near the surface. For the range of pressure ratios investigated, this condition was observed only for the nominal Mach 5.0 nozzle with the surface located at the downstream position of $x/d_j = 80$. These phenomena are covered in more detail in subsequent discussions along with sketches of the shocks and the resulting pressure distribution (figs. 5 to 8).

Tabulated Data

The pressure data obtained in this investigation are presented in tabular form and to a limited extent in graphical form. The data obtained from the $M_j = 1.0$ nozzle are presented in table I for separation distances from the nozzle exit to the surface of 20, 40, 80, 160, 240, and 400 nozzle-exit diameters and the data from the $M_j = 5.0$ nozzle are presented in table II for the separation distances from the nozzle exit to the surface of 4, 8, 20, 40, and 80 nozzle-exit diameters. Columns (1) to (5) of these tables present data as a nondimensional ratio of the surface static pressure to ambient pressure p_s/p_∞ for five constant values of the ratio of nozzle total pressure to ambient pressure p_t/p_∞ ranging from 50×10^3 to 250×10^3 . Columns (6) to (10) contain the identical data converted to ratios of surface static pressure to nozzle total pressure p_s/p_t . In general, data from the different pressure orifices located at the same radius indicate reasonably symmetrical pressure distributions for the higher surface pressures; somewhat larger deviations in the measured pressure at a particular radius occurred for the lower surface pressures (compare the tabulated data). The pressure-distribution curves included herein present only the data obtained along the vertical axis through $\psi = 0^\circ$ and $\psi = 180^\circ$, with the exception of figure 6(e) which presents all data as numerical averages for each radius.

Experimental Surface Pressure Distributions

The surface static-pressure distributions resulting from the impingement of exhaust plumes upon a flat surface are presented in figures 5 to 8. The abscissa of these figures extends over a range of r/d_j from 0 to 70 for $M_j = 1.0$ and from 0 to 14 for $M_j = 5.0$; this range is representative of the area of primary interest. One exception to this range

of r/d_j for which curves are shown is figure 6(e), which shows a typical variation of surface pressure out to the maximum radial positions for which data were obtained. For radial positions r/d_j larger than those shown in the other figures, refer to the tabulated data. The surface-pressure distributions are shown beginning at the impingement-surface center point and extending outward along the radial line through $\psi = 0^\circ$ and $\psi = 180^\circ$. Figure 6(e) presents all the data as numerical averages for each r/d_j value.

Ratio of surface static pressure to ambient pressure.- The ratios of the surface static pressure to the ambient pressure for the various ratios of nozzle total pressure to ambient pressure are presented in figures 5 and 6 for the $M_j = 1.0$ and $M_j = 5.0$ nozzles, respectively. Surface pressures produced by both test nozzles exhibited similar trends and resulted in systematic families of curves for the different nozzle total-pressure ratios. The highest values of surface static-pressure ratio p_s/p_∞ attained in this investigation for the $M_j = 1.0$ and $M_j = 5.0$ nozzles were 445 and 1880, respectively; these values were obtained at the two smallest separation distances and at the highest ratio of total pressure to ambient pressure. Peak surface pressures occur on the nozzle axis and decrease in a smooth continuous manner with increasing radial distance r/d_j as evidenced in figures 5(a), 5(b), 6(a), and 6(b) for the two smallest separation distances from the nozzle exit to the surface (the small irregularity of the $p_t/p_\infty = 50 \times 10^3$ curve in fig. 5(b) is discussed subsequently). The shock structure associated with this trend is a surface shock adjacent to the impingement surface which remains at a near constant standoff distance throughout the range of total-pressure ratios (type I shock formation shown in fig. 4).

As the separation distance increases, the general trend of the pressure distribution changes from a smooth continuous curve to an irregularly decreasing one as shown in figures 5(c) to 5(f) and figures 6(d) to 6(e). For the larger separation distances the peak pressures occur as an annulus about the axis rather than on the axis as previously indicated for the small separation distances. This change in pressure-distribution trend is probably the result of the change in the type of shock formation from a standoff surface shock (type I) to a type II shock formation shown in figure 4.

Also evident in figures 5(b), 6(c), and 6(d) at a pressure ratio of 50×10^3 is an increase in the pressure at $r/d_j \approx 64.0$, 10.5, and 12.5, respectively, which corresponds to the region of impingement of the plume boundary (refer to ordinates of fig. 3(a) at surface position II and fig. 3(b) at positions III and IV). A similar trend may have occurred at the other pressure ratios for these impingement-surface positions; however, insufficient pressure instrumentation at large radial locations prevented detection of this pressure rise. Figure 6(e) also shows this jump in surface pressure at the boundary-impingement points for each of the four highest nozzle pressure ratios; the theoretical plume boundary-impingement points are noted at the top of the figure. This rapid

increase is not an entirely unexpected phenomenon in view of the physical characteristics that exist within an exhaust plume as defined by the contours of theoretical Mach numbers. Radial Mach number distributions across an exhaust plume, at large values of x/d_j , show that between the plume internal shock and the jet boundary, local Mach numbers may be lower than those at the plume center line. Therefore, it might be speculated that higher pressures are possible in the region of the jet boundary.

Figure 6(e) shows yet another peculiarity in that a pressure increase exists over most of the surface at $p_t/p_\infty = 50 \times 10^3$. Schlieren photographs show that this phenomenon is associated with type III shock formations characterized by crossed oblique shocks followed by a surface shock. (A type III shock formation is shown in fig. 4.)

Ratio of surface static pressure to nozzle total pressure.- The ratio of the distributions of the surface static pressures to the nozzle total pressure p_s/p_t is presented in figures 7 and 8 for the $M_j = 1.0$ and $M_j = 5.0$ nozzles, respectively. For both nozzles at small to moderate separation distances (figs. 7(a) and 8(a)) a single curve represents the variation of the ratio of the surface static pressure to the nozzle total pressure for the entire range of pressure ratios investigated. The single curve obtained by averaging the narrow bands of data for the variation of p_s/p_t indicates, for these spacing ratios, that the surface pressures are directly proportional to the nozzle total pressure p_t and independent of p_t/p_∞ ; however, for large spacing ratios this trend does not necessarily hold true. A similar trend of constant surface pressures was observed for the impingement of exhaust plumes on adjacent parallel surfaces in reference 13. This phenomenon is a result of the fact that the plume internal characteristics for a region bounded by the internal shock and Mach disk at a given pressure ratio are not altered by increasing plume expansion (by increasing p_t/p_∞). The pressure distributions for the separation distances x/d_j of 80 and 20 shown in figures 7(a) and 8(a), respectively, are repeated in figures 7(b) and 8(b) in addition to the distributions for the larger separation distances. Since the surface pressures at large separation distances are relatively low, the ordinate scale has been greatly increased in these figures to show more clearly the effects of p_t/p_∞ on the radial pressure distributions. The data for separation distance x/d_j of 240 and 400 are not plotted in figure 7(b); however, the general trend of the curves would be somewhat similar to the data for $x/d_j = 160$. (See tables I and II.) The pressure increases shown in figure 8(b) at $r/d_j \approx 10.5$ and 12.5 for the separation distances of 20 and 40, respectively, are associated with the impingement of the plume boundaries as previously discussed. Also evident in figure 8(b) are higher pressures for $x/d_j = 80$ at $p_t/p_\infty = 50 \times 10^3$; the type of shock structure associated with this separation distance and pressure ratio is discussed in regard to the next two figures.

Figures 9 and 10 illustrate the shock-formation changes associated with the surface located 80 diameters downstream of the $M_j = 5.0$ nozzle. Presented in figure 9

are sketches representing the flow and shock structures within the exhaust plume as observed from the schlieren motion pictures at five different ratios of p_t/p_∞ . The two locations of the schlieren mirror represent two different tests from which the movies were correlated as accurately as possible by use of timing marks on the film strips and the p_t/p_∞ measurements. In the sketches for the three highest pressure ratios the shock structure consists primarily of a near-normal shock, or Mach disk, which moves upstream toward the nozzle exit and also decreases in diameter as the pressure ratio decreases. The absence of a surface shock in sketches (a) to (c) of figure 9 indicates that downstream of the normal shock the flow on the center line may not have expanded sufficiently to attain supersonic velocities. It is entirely possible, however, that the flow on the surface some distance away from the center may be supersonic but parallel to the surface and therefore without shocks. As the pressure ratio decreases from 81.25×10^3 (fig. 9; sketch (c)) to 67×10^3 (fig. 9; sketch (d)), the diameter of the Mach disk decreases until the Mach disk is eventually replaced by weak oblique (crossed) shocks with a surface shock adjacent to the impingement plate. Observation of the schlieren movies showed the change from the Mach disk to the oblique shock and associated surface shock to be rather instantaneous and to occur at a pressure ratio of approximately 67×10^3 . Sketch (d) represents the first frame of the movies where the oblique crossed shocks and surface shock combination first appeared; for further decreases in pressure ratio, the internal shock system becomes more clearly defined, as in sketch (e) of figure 9.

The change in surface pressure associated with the appearance of the oblique and normal shock structure is shown in figure 10 in the form of a continuous plot of the variation of the surface-pressure ratio with the nozzle total-pressure ratio. Although this figure presents only the pressure measured at the surface center-point orifice, it is typical of the pressure rise experienced by all static-pressure orifices located within a radius of approximately 16 nozzle-exit diameters. (See tables I and II). Figure 3(b) shows that this area is approximately equivalent to the maximum total area influenced by the jet plume for a ratio of nozzle total pressure to ambient pressure of about 67×10^3 . The lower-case letters at the top of figure 10 correspond to shock-structure sketches (a) to (e) of figure 9.

Figure 11 presents a comparison of the present data with data for the same type of nozzle from reference 7. Although the investigation of reference 7 was conducted for much smaller nozzle-to-surface separation distances than the present investigation, some overlapping of the test ranges did occur. In general, the agreement of the current data with data from reference 7 appears to be very good, particularly in the region where overlapping occurred.

Comparison of Experimental and Theoretical Data

Before estimations can be made of the effects produced by the impingement of highly expanded exhaust plumes on a surface, it is helpful to know certain facts about the plume internal characteristics. A useful tool in obtaining these plume internal characteristics is the method of characteristics. The characteristics program described in reference 14 and the interpolation program of reference 15 have been used to obtain the plume internal Mach number contours shown in figure 12. The contours for the exhaust plumes with $M_j = 1.0$ and $M_j = 4.79$ nozzles (figs. 12(a) and 12(b), respectively) are restricted to the regions of primary interest to this investigation. The contours for only one ratio of nozzle exit pressure to ambient pressure are shown since it has been previously noted that the contours bounded by the plume internal shock and Mach disk are unaffected by additional increases in pressure ratio. In figure 12(b) radial flow is assumed to exist between the leading characteristic line and the axial center line of the nozzle. (See ref. 14.)

Plume center-line Mach number.- The distributions of experimental and theoretical Mach numbers along the exhaust-plume axis are shown in figure 13(a). Experimental Mach number distributions were computed from normal-shock relations (ref. 16) by using the nozzle stagnation pressure and assuming the pressure measured by the surface center-point orifice at $p_t/p_\infty = 250 \times 10^3$ to be the total pressure behind a normal shock. It should be noted that the experimental data are plotted at the surface location. If these data were plotted at the surface-shock location, the symbols would be located at values of x/d_j slightly less than those shown. The present experimental data and those of reference 7 show good agreement for both nozzles in the region where overlapping of data exists. Theoretical values of center-line Mach number, obtained from the characteristic contour plots of figure 12, show satisfactory agreement with the experimental data for the $M_j = 1.0$ nozzle up to a Mach number of about 36. The agreement between theory and experimental data for the $M_j = 4.79$ nozzle was less satisfactory. For comparison purposes, the theoretical results for the $M_j = 5.0$, $\theta_n = 15^\circ$ inviscid-design nozzle are also shown.

The ratios of surface center-point pressures to the nozzle total pressures obtained experimentally and theoretically are shown in figure 13(b). The theoretical distributions of $p_{t,2}/p_{t,1}$ correspond to the theoretical Mach numbers shown in figure 13(a). Two theoretical curves are shown for each nozzle; one curve is based on the assumption that a normal shock occurs at the location of the impingement surface (this assumption was made in ref. 7), and the other curve represents the pressures obtained by accounting for the normal-shock standoff distance (ref. 17 uses this procedure). The latter assumption results in a lower Mach number M_1 and thus a larger value of $p_{t,2}/p_{t,1}$. The shock standoff distances were approximated by considering the mass balance through the shock

as was done in reference 3. The data for $M_j = 1.0$ appear to be well represented by the theoretical pressure distribution; however, a lack of agreement for the $M_j = 4.79$ data is evident for which no explanation is apparent.

Shock location. - The effects of the nozzle-pressure ratio and nozzle-to-surface separation distance on the downstream location of the Mach disk (l/d_j along the center line) are shown in figure 14. For convenience, the various impingement-surface locations are indicated by horizontally dashed lines. The figure also shows representative theoretical values of the Mach disk location with no impingement surface present in the plume; these curves were obtained by using the procedure found in reference 18. This method showed that a Mach disk would be formed at the location along the axial center line for which the pressure behind the shock is equal to the ambient pressure. The center-line Mach numbers for obtaining this approximation were obtained from the method of characteristics (as shown in fig. 12). Other methods for predicting the normal-shock location are contained in references 19 and 20. Also shown on figure 14(a) is a solid-line curve representing the experimental values for the location of the Mach disk for the $M_j = 1.0$ nozzle with no surface interference which were obtained from reference 14. The theoretical curves and the experimental curve are essentially linear variations of separation distance with pressure ratio when plotted on logarithmic scales. The approximation and the experimental curve are in good agreement for the $M_j = 1.0$ nozzle as shown in figure 14(a); experimental data were not available to make a similar comparison for the $M_j = 5.0$ nozzle.

The experimental data obtained in this investigation are represented in figure 14 by the symbols. The flagged symbols indicate data obtained during the investigation but not presented in the tables. The one solid symbol on figure 14(b) denotes crossed oblique shocks as shown in sketch (e) of figure 9. The general trend of the fairings indicates that as the pressure ratio is increased, the shock begins to deviate from the experimental location of reference 14 (no obstruction within the plume) and approaches the surface asymptotically. A standoff distance is finally reached at which further increases in the pressure ratio result in no change in the shock location. (The solid horizontal line represents calculated constant standoff shock locations obtained by using eq. (A18) of ref. 3.) Comparisons of the final standoff distance, at a pressure ratio of $p_j/p_\infty = 10^5$ (fig. 14(a)), for example, reveal that the surface-shock standoff distance decreases as the separation distance x/d_j decreases. By referring to figure 12 it is noted that the plume center-line Mach number decreases as the nozzle is approached, concurrent with the decreasing surface-shock standoff distance noted previously. This phenomenon is exactly opposite to the variation of a blunt-body bow-shock standoff distance which increases with decreasing stream Mach number. Shown in figure 14(b) for the surface locations x/d_j of 4 and 8 are some shock-standoff-distance data obtained from reference 9 which indicate good agreement with the present data.

Surface static-pressure distributions. - Comparisons of experimental and theoretical pressure distributions are presented in figure 15 to show the validity of determining the surface pressure distributions by theoretical methods. The method of reference 17 makes use of exhaust-plume internal characteristics such as those presented in figure 12. For a given plate location the position of the surface shock is determined either by measurements from schlieren photographs or by some theoretical method, and the shock shape is then superimposed on the characteristic Mach number contours. The pressure ratios $p_{t,2}/p_{t,1}$ are calculated from the Mach numbers associated with the Mach contours crossed by the superimposed surface shock. The resulting pressure ratios are then multiplied by the cosine squared of the angle the flow direction makes with the plume axis at the point where the surface shock crosses a Mach number contour. Also shown in these figures is an additional curve which was obtained by using the method described in reference 17 but assuming the shock to be located at and synonymous with the plate position and utilizing the Mach contours of figure 12. Although the surface pressure distributions obtained by the method of reference 17 compare favorably with experimental data, there are some apparent limitations in that prior knowledge of the plume internal characteristics, including the surface shock shape and location, is required.

The second method (ref. 3) is a simpler means of determining the pressure distribution in that only the exit Mach number and distance from the nozzle exit to the surface are required. Since this method is not applicable for low nozzle-exit Mach numbers, a comparison with experimental data is shown in figure 15 only for the $M_j = 5.0$ data. As indicated in the figure, this method shows the least agreement with the experimental data. References 3 and 9 show a much closer agreement between theory and experiment than is indicated in this investigation; however, in both references the nozzle was located much closer to the impingement surface than was shown in figure 15.

The methods of both references 3 and 17 assume that the pressure ratios p_t/p_∞ are high enough to assure a shock adjacent to the surface. For the $M_j = 1.0$ nozzle (fig. 15(a)) the surface is located sufficiently close to the nozzle exit to assure that the surface shock for the pressure ratio of 250×10^3 is at a constant standoff distance. Fair agreement of the theoretical and experimental pressure data is apparent for this standoff separation distance. However, for the $M_j = 5.0$ nozzle, also at a relatively close spacing (fig. 15(b)), the fair agreement of the experimental data with theory is less favorable on the plume axis, and better agreement exists a short distance from the axis.

Included at the top of figure 15 are the theoretical plume boundaries and internal shocks for both test nozzles at a pressure ratio of 250×10^3 . Also shown are the associated surface shocks. Reference 3 gives a method for determining the surface shock location and shape; however, the results agree with the current experimental shock-formation data only on the plume axis. Consequently, the shock formation shown used

the method of reference 3 only for finding the shock location on the axis; the remainder of the shock shape was approximated from the schlieren movies. Another analytical method for determining surface shock location and shape is presented in reference 21. A comparison of these two methods (refs. 3 and 21) was made in reference 9 and showed reasonable agreement of the surface shock shape on the plume axis; however, they deviated from one another at points farther from the center of impingement.

Postulated Shock Formations for a Lunar Landing

Since an actual lunar landing would probably be made with the nozzle-pressure ratio held constant as the vehicle approached the surface, it is of interest to know what kind of shock formation might be expected under these conditions. It is initially assumed that the separation distance is sufficiently large to prevent any influence on the Mach disk by the surface. In decreasing the separation distance the Mach disk approaches the impingement surface until some critical shock-standoff distance is reached where the Mach disk becomes what is termed herein as a surface shock. Continued descent essentially pushes the surface shock closer to the nozzle exit and slowly decreases the standoff distance between the shock and the surface. (See fig. 14.) Furthermore, decreasing the separation distance, at a constant pressure ratio, increases the maximum surface pressures and therefore greatly intensifies possible erosion problems.

SUMMARY OF RESULTS

An investigation has been conducted to determine the effects of highly underexpanded nozzle exhaust plumes impinging upon a flat surface placed perpendicular to the nozzle axis. The experimental tests were conducted in the Langley 41-foot-diameter vacuum sphere, and pressure measurements and high-speed schlieren photographs were obtained. Unheated air at a pressure of approximately 2400 psia (16.55×10^6 N/m²) was exhausted from two different nozzles, a converging nozzle (with an exit Mach number of 1.0) and a converging-diverging nozzle (with a nominal design exit Mach number of 5.0). The results obtained in the investigation are as follows:

1. Three shock formations were found to exist which were dependent upon the distance from the nozzle exit to the impingement surface and the ratio of the nozzle total pressure to ambient pressure. The most frequently observed shock formation in these tests consisted of a surface shock located at a standoff distance from the surface which remained constant over a large range of pressure ratios; this condition was predominant for relatively small distances from the nozzle exit to the surface. For large separation distances the surface shock acts similar to a Mach disk but is located closer to the nozzle

exit than it would normally be if no surface were present in the plume; the shock standoff distance from the surface increases as the pressure ratio decreases. The third shock formation is evident for larger separation distances and low pressure ratios and is characterized by crossed oblique shocks followed by a surface shock adjacent to the plate.

2. When the distances between the nozzle exit and the surface were small, the surface pressures produced by both nozzles exhibited similar trends over the range of nozzle total-pressure ratios investigated; maximum surface pressures occurred on the nozzle axis and decreased in a smooth continuous manner with increasing radial distance. A single-curve representation of the variation of the ratio of surface static pressure to nozzle total pressure showed the surface pressure to be directly proportional to the nozzle total pressure and independent of the ratio of nozzle total pressure to ambient pressure for low and medium nozzle separation distances.

3. For large separation distances, the maximum pressures occurred as an annulus about the axis; at the same time the radial pressure distribution changed from a smoothly decreasing curve to one with some oscillations. Under some test conditions maximum surface pressures were recorded near the plume-boundary impingement location.

4. As the ratio of nozzle total pressure to ambient pressure was decreased for the Mach 5.0 nozzle located at the largest separation distance, a crossed oblique shock formation occurred instantaneously with an associated normal shock adjacent to the surface. This shock formation was accompanied by an instantaneous increase in pressure over all the surface area influenced by the plume impingement.

5. Experimental and theoretical center-line Mach number distributions for the Mach 1.0 nozzle were in good agreement up to a plume center-line Mach number of about 36. The agreement between theoretical and experimental data for the nominal Mach 5.0 nozzle was less satisfactory.

6. Semiempirically calculated impingement-surface pressures (prior knowledge of the shock shape being necessary) compare favorably with experimental data. Use of a much simpler theoretical method of obtaining the surface pressures resulted in somewhat less favorable agreement with the experimental data.

Langley Research Center,
National Aeronautics and Space Administration,
Langley Station, Hampton, Va., October 9, 1965.

APPENDIX

CONVERSION OF U.S. CUSTOMARY UNITS TO SI UNITS

The International System of Units (SI) was adopted by the Eleventh General Conference on Weights and Measures, Paris, October 1960, in Resolution No. 12 (ref. 12). Conversion factors for the units used herein are given in the following table:

Physical quantity	U.S. Customary Unit	Conversion factor (*)	SI Unit
Length	in.	0.0254	meters (m)
Pressure	psi = lbf/in ²	6894.7	newton/meter ² (N/m ²)
Pressure	torr (0° C)	133.32	newton/meter ² (N/m ²)
Temperature	°F + 459.67	5/9	degrees Kelvin (°K)

*Multiply value given in U.S. Customary Unit by conversion factor to obtain equivalent value in SI unit.

REFERENCES

1. Vick, Allen R.; Cabbage, James M.; and Andrews, Earl H., Jr.: Rocket Exhaust Plume Problems and Some Recent Related Research. Presented at a Specialists' Meeting on "The Fluid Dynamic Aspects of Space Flight" (Marseille, France), AGARD, April 20-24, 1964.
2. Binion, T. W., Jr.: Jet Interference During Stage Separation at Very High Altitudes. AEDC-TDR-64-89, U.S. Air Force, May 1964.
3. Roberts, Leonard: The Action of a Hypersonic Jet on a Dust Layer. Paper No. 63-50, Inst. Aerospace Sci., Jan. 1963.
4. Cramblit, D. C.: A Consideration of Lunar Surface Ballistics and the Hazards Associated With Spacecraft Landing or Launch Operations. NASA TN D-1526, 1963.
5. Shepard, Dudley C.: The Effect of Retro-Rocket Exhaust on Visibility During Lunar Touchdown. Rept. No. 391 (Contract NAS9-153), M.I.T., Dec. 1962.
6. Sibulkin, M.; and Gallaher, W. H.: Some Aspects of the Interaction of a Jet With a Dust Covered Surface in a Vacuum Environment. Rept. ERR-AN-244 (Contract No. REA 111-9403), Eng. Dept., Gen. Dyn./Astronaut., Feb. 10, 1963.
7. Stitt, Leonard E.: Interaction of Highly Underexpanded Jets With Simulated Lunar Surfaces. NASA TN D-1095, 1961.
8. Spady, Amos A., Jr.: An Exploratory Investigation of Jet-Blast Effects on a Dust-Covered Surface at Low Ambient Pressure. NASA TN D-1017, 1962.
9. Land, Norman S.; and Clark, Leonard V.: Experimental Investigation of Jet Impingement on Surfaces of Fine Particles in a Vacuum Environment. NASA TN D-2633, 1965.
10. Hurt, George J., Jr.; and Lina, Lindsay J.: Blast Effects of Twin Variable-Cant Rocket Nozzles on Visibility During Landing on a Particle-Covered Surface. NASA TN D-2455, 1964.
11. Fergus, J. L., Jr.; and Gall, E. S.: Techniques Used to Test Small Rocket Engines at Near Space Conditions. Paper No. 64-203, Am. Inst. Aeron. Astronaut., June 1964.
12. Mechtly, E. A.: The International System of Units - Physical Constants and Conversion Factors. NASA SP-7012, 1964.
13. Vick, Allen R.; and Andrews, Earl H., Jr.: An Experimental Investigation of Highly Underexpanded Free Jets Impinging Upon a Parallel Flat Surface. NASA TN D-2336, 1964.

14. Vick, Allen R.; Andrews, Earl H., Jr.; Dennard, John S., and Craidon, Charlotte B.: Comparisons of Experimental Free-Jet Boundaries With Theoretical Results Obtained With the Method of Characteristics. NASA TN D-2327, 1964.
15. Andrews, Earl H., Jr.; Vick, Allen R.; and Craidon, Charlotte B.: Theoretical Boundaries and Internal Characteristics of Exhaust Plumes From Three Different Supersonic Nozzles. NASA TN D-2650, 1965.
16. Ames Research Staff: Equations, Tables, and Charts for Compressible Flow. NACA Rept. 1135, 1953. (Supersedes NACA TN 1428.)
17. Eastman, Donald W.; and Radtke, Leonard P.: Flow Field of an Exhaust Plume Impinging on a Simulated Lunar Surface. AIAA J., vol. 1, no. 6, June 1963, pp. 1430-1431.
18. Adamson, Thomas C., Jr.: The Structure of the Rocket Exhaust Plume Without Reaction at Various Altitudes. 4613-45-T (Contract SD-91), Inst. Sci. Technol., Univ. of Michigan, June 1963.
19. Eastman, Donald W.; and Radtke, Leonard P.: Location of the Normal Shock Wave in the Exhaust Plume of a Jet. AIAA J. (Tech. Notes and Comments), vol. 1, no. 4, Apr. 1963, pp. 918-919.
20. D'Attorre, L.; and Harshbarger, F.: Experimental and Theoretical Studies of Underexpanded Jets Near the Mach Disc. GDA-DBE 64-008 (Contract No. AF 19(628)-3269), Gen. Dyn./Astronaut., Feb. 19, 1964.
21. Edwards, R. H.: Interaction of the Surveyor Vernier Rocket With the Surface of the Moon. Hughes Aircraft Co., IDC Ref. 4162.1/34, Apr. 12, 1961.

TABLE I - SURFACE-PRESSURE-DATA RESULTS OF $M_j = 1.0$ NOZZLE EXHAUST PLUME
IMPINGING UPON A PERPENDICULAR FLAT SURFACE

(a) $x/d_j = 20$

Orifice	r/d_j	ψ , deg	P_s/P_∞ for values of P_t/P_∞ of -					P_s/P_t for values of P_t/P_∞ of -				
			①	②	③	④	⑤	⑥	⑦	⑧	⑨	⑩
			50×10^3	100×10^3	150×10^3	200×10^3	250×10^3	50×10^3	100×10^3	150×10^3	200×10^3	250×10^3
1	0	---	88.0	180.0	270.0	357.0	445.0	1.760×10^{-3}	1.800×10^{-3}	1.800×10^{-3}	1.785×10^{-3}	1.780×10^{-3}
2	4	0	---	---	---	---	---	---	---	---	---	---
3	8	0	59.0	120.0	180.0	238.0	296.0	1.180	1.200	1.200	1.190	1.184
4	8	90	57.0	115.0	172.0	229.0	286.0	1.140	1.150	1.147	1.145	1.144
5	8	180	57.0	115.0	172.0	229.0	286.0	1.140	1.150	1.147	1.145	1.144
6	8	270	59.0	120.0	180.0	238.0	296.0	1.180	1.200	1.200	1.190	1.184
7	16	0	21.0	44.0	67.0	88.0	110.0	.420	.440	.447	.440	.440
8	16	45	21.0	44.0	67.0	88.0	110.0	.420	.440	.447	.440	.440
9	16	135	20.0	42.0	63.0	84.0	105.0	.400	.420	.420	.420	.420
10	16	180	20.0	42.0	63.0	84.0	105.0	.400	.420	.420	.420	.420
11	16	225	20.0	42.0	63.0	84.0	105.0	.400	.420	.420	.420	.420
12	16	315	20.0	42.0	63.0	84.0	105.0	.400	.420	.420	.420	.420
13	24	0	6.40	13.70	20.60	27.10	33.50	.128	.137	.137	.136	.134
14	32	0	2.30	5.80	9.00	12.20	15.40	.046	.058	.060	.061	.062
15	32	90	2.30	5.20	8.00	10.60	13.30	.046	.052	.053	.053	.053
16	48	0	.20	1.40	2.30	3.00	3.70	.004	.014	.015	.015	.015
17	48	45	.20	1.10	2.00	2.80	3.70	.004	.011	.013	.014	.015
18	64	0	.20	.50	.90	1.10	1.40	.004	.005	.006	.006	.006
19	64	90	.20	.50	1.00	1.40	1.90	.004	.005	.007	.007	.008
20	80	45	---	.32	.53	.68	.81	---	.003	.004	.003	.003
21	96	0	---	.50	.70	.70	.70	---	.005	.005	.004	.003
22	96	90	---	.50	.70	.70	.70	---	.005	.005	.004	.003
23	112	45	.33	.43	.70	.76	.83	.007	.004	.005	.004	.003
24	128	0	.77	.42	.81	.74	.68	.015	.004	.005	.004	.003
25	128	90	.70	.61	.86	.83	.80	.014	.006	.006	.004	.003
26	144	45	.85	.43	.82	.83	.84	.017	.004	.005	.004	.003
27	160	0	.36	.64	.76	.76	.75	.007	.006	.005	.004	.003
28	176	45	---	1.09	.86	.83	.79	---	.011	.006	.004	.003

(b) $x/d_j = 40$

Orifice	r/d_j	ψ , deg	P_s/P_∞ for values of P_t/P_∞ of -					P_s/P_t for values of P_t/P_∞ of -				
			①	②	③	④	⑤	⑥	⑦	⑧	⑨	⑩
			50×10^3	100×10^3	150×10^3	200×10^3	250×10^3	50×10^3	100×10^3	150×10^3	200×10^3	250×10^3
1	0	---	20.5	42.5	64.5	86.1	107.7	0.410×10^{-3}	0.425×10^{-3}	0.430×10^{-3}	0.431×10^{-3}	0.431×10^{-3}
2	4	0	20.1	41.2	61.7	82.1	102.5	.402	.412	.411	.410	.410
3	8	0	18.8	38.3	57.5	76.8	95.8	.376	.383	.383	.384	.383
4	8	90	18.7	38.3	58.5	77.8	97.0	.374	.383	.390	.389	.388
5	8	180	19.5	39.5	59.4	78.8	98.2	.390	.395	.396	.394	.393
6	8	270	19.2	38.8	58.5	77.5	96.7	.384	.388	.390	.388	.387
7	16	0	12.9	27.0	41.0	55.0	69.0	.258	.270	.273	.275	.276
8	16	45	12.3	26.0	40.4	54.2	68.0	.246	.260	.269	.271	.272
9	16	135	13.8	27.7	41.8	55.7	69.6	.276	.277	.279	.279	.278
10	16	180	12.3	26.0	40.6	55.4	69.6	.246	.260	.271	.277	.278
11	16	225	14.2	29.2	44.3	59.2	74.2	.284	.292	.295	.296	.297
12	16	315	13.4	27.7	42.2	56.7	71.2	.268	.277	.281	.284	.285
13	24	0	8.6	17.5	26.4	35.2	44.0	.172	.175	.176	.176	.176
14	32	0	4.9	10.4	15.9	21.4	26.8	.098	.104	.106	.107	.107
15	32	90	4.80	9.90	15.25	20.40	25.50	.096	.099	.102	.102	.102
16	48	0	1.60	3.40	5.50	7.50	9.50	.032	.034	.037	.038	.038
17	48	45	1.00	5.00	5.10	7.15	3.30	.020	.030	.034	.036	.037
18	64	0	2.50	1.40	2.30	3.30	4.30	.050	.014	.015	.017	.017
19	64	90	2.50	1.10	2.00	3.00	3.90	.050	.011	.013	.015	.016
20	80	45	1.40	1.63	1.08	1.37	1.68	.028	.016	.007	.007	.007
21	96	0	.37	1.28	1.08	.92	1.24	.007	.013	.007	.005	.005
22	96	90	.37	1.28	1.08	.92	1.24	.007	.013	.007	.005	.005
23	112	45	.47	.64	1.00	.74	.68	.009	.006	.007	.004	.003
24	128	0	.69	.54	.73	.89	.98	.014	.005	.005	.004	.004
25	128	90	.78	.83	.73	.89	.98	.016	.008	.005	.004	.004
26	144	45	1.09	.61	.72	.71	.70	.022	.006	.005	.004	.003
27	160	0	.90	.73	.85	.97	1.09	.018	.007	.006	.005	.004
28	176	45	.17	.84	.78	.88	.98	.003	.008	.005	.004	.004

TABLE I.- SURFACE-PRESSURE-DATA RESULTS OF $M_j = 1.0$ NOZZLE EXHAUST PLUME
IMPINGING UPON A PERPENDICULAR FLAT SURFACE - Continued

(c) $x/d_j = 80$

Orifice	r/d_j	ψ , deg	P_s/P_∞ for values of P_t/P_∞ of -					P_s/P_t for values of P_t/P_∞ of -				
			P_t/P_∞ of -					P_t/P_∞ of -				
			50×10^3	100×10^3	150×10^3	200×10^3	250×10^3	50×10^3	100×10^3	150×10^3	200×10^3	250×10^3
1	0	---	4.40	8.80	13.50	18.20	22.90	0.088 × 10 ⁻³	0.088 × 10 ⁻³	0.090 × 10 ⁻³	0.091 × 10 ⁻³	0.092 × 10 ⁻³
2	4	0	4.60	9.70	14.90	20.10	25.40	.092	.097	.099	.101	.102
3	8	0	4.75	9.70	14.80	19.75	24.70	.095	.097	.099	.099	.102
4	8	90	4.60	9.75	15.10	20.50	25.90	.092	.098	.101	.103	.104
5	8	180	4.75	9.40	14.40	19.40	24.40	.095	.094	.096	.097	.098
6	8	270	4.75	9.70	14.80	19.75	24.70	.095	.097	.099	.099	.099
7	16	0	3.80	8.10	12.90	17.75	22.65	.076	.081	.086	.089	.091
8	16	45	3.60	8.10	13.55	19.10	24.15	.072	.081	.090	.091	.097
9	16	135	4.40	8.80	13.20	17.60	22.00	.088	.088	.088	.088	.088
10	16	180	3.10	7.00	11.70	16.75	21.70	.062	.070	.078	.084	.087
11	16	225	4.40	9.00	14.00	19.10	24.28	.088	.090	.093	.096	.097
12	16	315	4.00	8.45	13.65	19.00	24.33	.080	.085	.091	.095	.097
13	24	0	3.77	7.37	11.33	15.25	19.20	.075	.074	.076	.076	.077
14	32	0	3.60	6.90	10.65	14.35	18.06	.072	.069	.071	.072	.072
15	32	90	3.60	6.73	10.28	13.76	17.30	.072	.067	.069	.069	.069
16	48	0	2.74	4.08	6.45	9.00	11.55	.055	.041	.043	.045	.046
17	48	45	2.15	3.77	6.10	8.87	11.13	.043	.038	.041	.044	.045
18	64	0	2.33	2.32	3.76	5.35	6.65	.047	.023	.025	.027	.027
19	64	90	1.86	1.90	3.35	5.00	6.35	.037	.019	.022	.025	.025
20	80	45	2.22	2.74	2.30	3.20	4.10	.044	.027	.015	.016	.016
21	96	0	1.30	2.80	2.35	1.80	2.00	.026	.028	.016	.009	.008
22	96	90	1.30	2.80	2.35	1.80	2.00	.026	.028	.016	.009	.008
23	112	45	.68	2.05	2.36	1.67	1.17	.014	.020	.016	.008	.005
24	128	0	.55	1.13	2.35	2.44	1.44	.011	.011	.016	.012	.006
25	128	90	.77	1.43	3.11	3.37	2.23	.015	.014	.021	.017	.009
26	144	45	.71	.60	1.44	2.05	2.28	.014	.006	.010	.010	.009
27	160	0	1.00	.81	.81	1.28	1.76	.020	.008	.005	.006	.007
28	176	45	.16	.48	.71	.62	.56	.003	.005	.005	.003	.002

(d) $x/d_j = 160$

Orifice	r/d_j	ψ , deg	P_s/P_∞ for values of P_t/P_∞ of -					P_s/P_t for values of P_t/P_∞ of -				
			P_t/P_∞ of -					P_t/P_∞ of -				
			50×10^3	100×10^3	150×10^3	200×10^3	250×10^3	50×10^3	100×10^3	150×10^3	200×10^3	250×10^3
1	0	---	1.27	1.76	2.44	3.33	4.25	0.025 × 10 ⁻³	0.018 × 10 ⁻³	0.016 × 10 ⁻³	0.017 × 10 ⁻³	0.017 × 10 ⁻³
2	4	0	1.75	2.56	3.55	4.63	5.63	.035	.026	.024	.023	.023
3	8	0	1.86	2.72	3.75	4.78	5.82	.037	.027	.025	.024	.023
4	8	90	1.66	2.50	3.54	4.65	5.70	.033	.025	.024	.023	.023
5	8	180	1.78	2.66	3.67	4.80	5.74	.036	.027	.024	.024	.023
6	8	270	1.83	2.72	3.70	4.70	5.70	.037	.027	.025	.024	.023
7	16	0	1.43	2.20	3.26	4.45	5.57	.029	.022	.022	.022	.022
8	16	45	1.27	2.24	3.51	4.96	6.30	.025	.022	.023	.025	.025
9	16	135	1.85	2.70	3.62	4.58	5.44	.037	.027	.024	.023	.022
10	16	180	.66	1.54	2.94	4.14	5.47	.013	.015	.020	.021	.022
11	16	225	1.77	2.76	3.87	5.22	6.10	.035	.028	.026	.026	.024
12	16	315	1.28	2.22	3.38	4.73	5.92	.026	.022	.023	.024	.024
13	24	0	1.80	2.50	3.30	4.14	4.88	.036	.025	.022	.021	.020
14	32	0	1.86	2.80	3.80	4.70	5.50	.037	.028	.025	.024	.022
15	32	90	1.86	2.64	3.53	4.38	5.15	.037	.026	.024	.022	.021
16	48	0	1.62	2.40	3.24	4.06	4.78	.032	.024	.022	.020	.019
17	48	45	1.20	2.00	3.00	3.76	4.47	.024	.020	.020	.019	.018
18	64	0	1.60	2.20	2.94	3.54	4.07	.032	.022	.020	.018	.016
19	64	90	1.20	1.80	2.58	3.32	3.77	.024	.018	.017	.017	.015
20	80	45	1.81	2.23	2.71	3.18	3.66	.036	.022	.018	.016	.015
21	96	0	1.50	1.85	2.30	2.75	3.00	.030	.019	.015	.014	.012
22	96	90	1.80	2.10	2.40	2.75	3.00	.036	.021	.016	.014	.012
23	112	45	1.68	1.93	2.20	2.48	2.75	.034	.019	.015	.012	.011
24	128	0	1.29	1.97	2.29	2.57	2.88	.026	.020	.015	.013	.012
25	128	90	1.19	1.82	2.09	2.34	2.60	.024	.018	.014	.012	.010
26	144	45	.88	1.85	2.27	2.40	2.54	.018	.018	.015	.012	.010
27	160	0	.75	1.29	1.81	2.13	2.42	.015	.013	.012	.011	.010
28	176	45	.21	.40	1.04	1.76	2.50	.004	.004	.007	.009	.010

TABLE I.- SURFACE-PRESSURE-DATA RESULTS OF $M_j = 1.0$ NOZZLE EXHAUST PLUME
IMPINGING UPON A PERPENDICULAR FLAT SURFACE - Concluded

(e) $x/d_j = 240$

Orifice	r/d_j	ψ , deg	P_s/P_∞ for values of P_t/P_∞ of -					P_s/P_t for values of P_t/P_∞ of -					⑩
			P_t/P_∞ of -					P_t/P_∞ of -					
			50×10^3	100×10^3	150×10^3	200×10^3	250×10^3	50×10^3	100×10^3	150×10^3	200×10^3	250×10^3	
1	0	---	0.840	0.861	1.010	1.292	1.600	0.017×10^{-3}	0.009×10^{-3}	0.007×10^{-3}	0.006×10^{-3}	0.006×10^{-3}	
2	4	0	1.180	1.494	1.743	1.981	2.220	.024	.015	.012	.010	.009	
3	8	0	1.357	1.750	2.076	2.423	2.773	.027	.018	.014	.012	.011	
4	8	90	1.235	1.587	1.875	2.155	2.440	.025	.016	.012	.011	.010	
5	8	180	1.360	1.720	2.010	2.340	2.660	.027	.017	.013	.012	.011	
6	8	270	1.450	1.920	2.285	2.663	3.042	.029	.019	.015	.013	.012	
7	16	0	.911	1.223	1.613	2.010	2.430	.018	.012	.011	.010	.010	
8	16	45	.762	1.348	1.980	2.585	3.192	.015	.013	.013	.013	.013	
9	16	135	1.470	1.800	2.113	2.426	2.735	.029	.018	.014	.012	.011	
10	16	180	.500	1.053	1.675	2.228	2.760	.010	.011	.011	.011	.011	
11	16	225	1.200	1.660	2.085	2.510	2.940	.024	.017	.014	.013	.012	
12	16	315	.960	1.500	2.030	2.564	3.100	.019	.015	.014	.013	.012	
13	24	0	1.408	1.753	2.088	2.423	2.760	.028	.018	.014	.012	.011	
14	32	0	1.452	1.977	2.434	2.815	3.132	.029	.020	.016	.014	.013	
15	32	90	1.483	1.885	2.205	2.526	2.845	.030	.019	.015	.013	.011	
16	48	0	1.280	1.723	2.075	2.430	2.783	.026	.017	.014	.012	.011	
17	48	45	.831	1.323	1.753	2.160	2.563	.017	.013	.012	.011	.010	
18	64	0	1.312	1.668	1.955	2.245	2.538	.026	.017	.013	.011	.010	
19	64	90	.932	1.311	1.673	2.066	2.453	.019	.013	.011	.010	.010	
20	80	45	1.483	1.827	2.040	2.253	2.468	.030	.018	.014	.011	.010	
21	96	0	1.540	1.580	1.850	2.020	2.100	.031	.016	.012	.010	.008	
22	96	90	1.880	1.800	2.000	2.200	2.330	.038	.018	.013	.011	.009	
23	112	45	1.925	1.700	1.750	1.825	1.900	.038	.017	.012	.009	.008	
24	128	0	1.925	1.950	1.950	1.990	2.025	.038	.020	.013	.010	.008	
25	128	90	1.440	1.625	1.550	1.680	1.800	.029	.016	.010	.008	.007	
26	144	45	1.150	1.890	1.880	1.920	1.970	.023	.019	.013	.010	.008	
27	160	0	.900	1.535	1.660	1.700	1.750	.018	.015	.011	.008	.007	
28	176	45	0	.750	1.530	1.725	1.800	0	.008	.010	.009	.007	

(f) $x/d_j = 400$

Orifice	r/d_j	ψ , deg	P_s/P_∞ for values of P_t/P_∞ of -					P_s/P_t for values of P_t/P_∞ of -					⑩
			P_t/P_∞ of -					P_t/P_∞ of -					
			50×10^3	100×10^3	150×10^3	200×10^3	250×10^3	50×10^3	100×10^3	150×10^3	200×10^3	250×10^3	
1	0	---	0.768	0.890	1.075	1.260	---	0.015×10^{-3}	0.009×10^{-3}	0.007×10^{-3}	0.006×10^{-3}	---	
2	4	0	1.053	1.250	1.459	1.668	---	.021	.012	.010	.008	---	
3	8	0	1.126	1.331	1.547	1.763	---	.023	.013	.010	.009	---	
4	8	90	1.014	1.163	1.347	1.528	---	.020	.012	.009	.013	---	
5	8	180	1.092	1.250	1.459	1.668	---	.022	.012	.010	.008	---	
6	8	270	1.150	1.331	1.547	1.763	---	.023	.013	.010	.009	---	
7	16	0	.910	1.170	1.496	1.820	---	.018	.012	.010	.009	---	
8	16	45	.800	1.120	1.480	1.841	---	.016	.011	.010	.009	---	
9	16	135	1.138	1.282	1.458	1.632	---	.023	.013	.010	.008	---	
10	16	180	.580	.950	1.351	1.754	---	.012	.010	.009	.009	---	
11	16	225	1.114	1.350	1.629	1.906	---	.022	.013	.011	.010	---	
12	16	315	.898	1.210	1.573	1.932	---	.018	.012	.010	.010	---	
13	24	0	1.070	1.281	1.512	1.744	---	.021	.013	.010	.009	---	
14	32	0	1.190	1.443	1.736	2.030	---	.024	.014	.012	.010	---	
15	32	90	1.175	1.298	1.448	1.600	---	.024	.013	.010	.008	---	
16	48	0	1.090	1.377	1.734	2.091	---	.022	.014	.012	.010	---	
17	48	45	---	---	---	---	---	---	---	---	---	---	
18	64	0	1.084	1.293	1.531	1.764	---	.022	.013	.010	.009	---	
19	64	90	.830	1.088	1.362	1.636	---	.017	.011	.009	.008	---	
20	80	45	1.200	1.358	1.562	1.768	---	.024	.014	.010	.009	---	
21	96	0	1.320	1.400	1.470	1.550	---	.026	.014	.010	.008	---	
22	96	90	---	---	---	---	---	---	---	---	---	---	
23	112	45	1.400	1.460	1.530	1.600	---	.028	.015	.010	.008	---	
24	128	0	1.600	1.680	1.710	1.730	---	.032	.017	.011	.009	---	
25	128	90	1.260	1.530	1.530	1.500	---	.025	.015	.010	.008	---	
26	144	45	1.425	1.880	2.140	2.400	---	.028	.019	.014	.012	---	
27	160	0	1.180	1.580	1.950	2.320	---	.024	.016	.013	.012	---	
28	176	45	.400	1.170	1.700	2.230	---	.008	.012	.011	.011	---	

TABLE II. - SURFACE-PRESSURE-DATA RESULTS OF $M_j = 5.0$ NOZZLE EXHAUST PLUME
IMPINGING UPON A PERPENDICULAR FLAT SURFACE

(a) $x/d_j = 4$

Orifice	r/d_j	ψ , deg	P_s/P_∞ for values of P_t/P_∞ of -					P_s/P_t for values of P_t/P_∞ of -				
			①	②	③	④	⑤	⑥	⑦	⑧	⑨	⑩
			50×10^3	100×10^3	150×10^3	200×10^3	250×10^3	50×10^3	100×10^3	150×10^3	200×10^3	250×10^3
1	0	1	376	750	1127	1499	1880	7.520×10^{-3}	7.500×10^{-3}	7.510×10^{-3}	7.500×10^{-3}	7.520×10^{-3}
2	.8	0	225	460	700	944	1190	4.500	4.600	4.670	4.720	4.760
3	1.6	0	100	202	304	407	509	2.000	2.015	2.027	2.035	2.036
4	1.6	90	100	198	296	391	481	2.000	1.980	1.973	1.953	1.924
5	1.6	180	120	241	362	482	597	2.400	2.410	2.413	2.410	2.388
6	1.6	270	86	170	254	338	422	1.720	1.700	1.693	1.690	1.688
7	3.2	0	17.0	35.0	55.0	75.0	97.5	.340	.350	.367	.350	.390
8	3.2	45	17.0	35.0	55.0	75.0	97.5	.340	.350	.367	.350	.390
9	3.2	135	17.0	35.0	55.0	75.0	97.5	.340	.350	.367	.350	.390
10	3.2	180	17.0	35.0	55.0	75.0	97.5	.340	.350	.367	.350	.390
11	3.2	225	17.0	35.0	55.0	75.0	97.5	.340	.350	.367	.350	.390
12	3.2	315	17.0	35.0	55.0	75.0	97.5	.340	.350	.367	.350	.390
13	4.8	0	3.94	8.22	12.67	17.14	21.82	.079	.082	.084	.086	.087
14	6.4	0	1.90	3.31	4.90	6.51	8.03	.038	.033	.033	.033	.032
15	6.4	90	1.00	2.29	3.88	5.39	6.98	.020	.023	.026	.027	.028
16	9.6	0	.45	.75	1.07	1.53	1.67	.009	.008	.007	.008	.007
17	9.6	45	.45	.75	1.07	1.38	1.67	.009	.008	.007	.007	.007
18	12.8	0	.40	.60	.58	.62	.82	.008	.006	.004	.003	.003
19	12.8	90	.40	.60	.58	.62	.82	.008	.006	.004	.003	.003
20	16	45	.40	.75	.80	.80	.80	.008	.008	.005	.004	.003
21	19.2	0	.45	.71	.82	.92	.92	.009	.007	.005	.005	.004
22	19.2	90	.73	.82	.90	.92	.92	.015	.008	.006	.005	.004
23	22.4	45	.63	.78	.83	.88	.90	.013	.008	.006	.004	.004
24	25.6	0	.72	.78	.81	.78	.80	.014	.008	.005	.004	.003
25	25.6	90	.66	.78	.81	.88	.91	.013	.008	.005	.004	.004
26	28.8	45	.70	.80	.85	.90	.90	.014	.008	.006	.004	.004
27	32.0	0	.32	.71	.75	.80	.82	.006	.007	.005	.004	.003
28	35.2	45	.57	.64	.75	.80	.82	.011	.006	.005	.004	.003

(b) $x/d_j = 8$

Orifice	r/d_j	ψ , deg	P_s/P_∞ for values of P_t/P_∞ of -					P_s/P_t for values of P_t/P_∞ of -				
			①	②	③	④	⑤	⑥	⑦	⑧	⑨	⑩
			50×10^3	100×10^3	150×10^3	200×10^3	250×10^3	50×10^3	100×10^3	150×10^3	200×10^3	250×10^3
1	0	---	93.0	186.0	278.0	368.0	458.0	1.860×10^{-3}	1.860×10^{-3}	1.853×10^{-3}	1.840×10^{-3}	1.832×10^{-3}
2	.8	0	---	---	---	---	---	---	---	---	---	---
3	1.6	0	56.0	113.0	171.0	229.0	287.0	1.120	1.130	1.140	1.145	1.148
4	1.6	90	56.0	113.0	169.0	224.0	280.0	1.120	1.130	1.127	1.120	1.120
5	1.6	180	58.0	117.0	177.0	238.0	300.0	1.160	1.170	1.180	1.190	1.200
6	1.6	270	58.0	117.0	177.0	236.0	295.0	1.160	1.170	1.180	1.180	1.180
7	3.2	0	25.0	52.0	79.0	106.0	133.0	.500	.520	.527	.530	.532
8	3.2	45	25.0	50.5	76.0	102.0	128.0	.500	.505	.507	.510	.512
9	3.2	135	25.0	52.0	79.0	106.0	133.0	.500	.520	.527	.530	.532
10	3.2	180	25.0	52.0	79.0	106.0	133.0	.500	.520	.527	.530	.532
11	3.2	225	25.0	52.0	79.0	106.0	133.0	.500	.520	.527	.530	.532
12	3.2	315	25.0	52.0	79.0	106.0	133.0	.500	.520	.527	.530	.532
13	4.8	0	11.50	22.90	34.20	45.20	56.00	.230	.229	.228	.226	.224
14	6.4	0	5.00	10.00	14.90	19.80	24.80	.100	.100	.099	.099	.099
15	6.4	90	5.00	10.00	14.90	19.80	24.80	.100	.100	.099	.099	.099
16	9.6	0	1.30	3.20	3.60	4.90	6.25	.026	.032	.024	.025	.025
17	9.6	45	1.30	3.20	3.60	4.90	6.25	.026	.032	.024	.025	.025
18	12.8	0	.20	.80	1.40	1.60	1.80	.004	.008	.009	.008	.007
19	12.8	90	.20	.80	1.40	1.60	1.80	.004	.008	.009	.008	.007
20	16	45	.20	.50	.65	.70	.80	.004	.005	.004	.004	.003
21	19.2	0	.20	.78	.84	.89	.94	.004	.008	.006	.004	.004
22	19.2	90	.35	.98	.98	.98	.99	.007	.010	.007	.005	.004
23	22.4	45	.20	.74	.80	.80	.80	.004	.007	.005	.004	.003
24	25.6	0	.33	.80	.83	.87	.90	.007	.008	.006	.004	.004
25	25.6	90	.40	.80	.83	.87	.90	.008	.008	.006	.004	.004
26	28.8	45	1.38	.79	.86	.92	.98	.028	.008	.006	.005	.004
27	32.0	0	1.05	.62	.74	.78	.82	.021	.006	.005	.004	.003
28	35.2	45	.61	.70	.82	.87	.92	.012	.007	.005	.004	.004

TABLE II - SURFACE-PRESSURE-DATA RESULTS OF $M_j = 5.0$ NOZZLE EXHAUST PLUME
IMPINGING UPON A PERPENDICULAR FLAT SURFACE - Continued

(c) $x/d_j = 20$

Orifice	r/d _j	ψ, deg	P _s /P _∞ for values of P _t /P _∞ of -					P _s /P _t for values of P _t /P _∞ of -				
			①	②	③	④	⑤	⑥	⑦	⑧	⑨	⑩
			50 × 10 ³	100 × 10 ³	150 × 10 ³	200 × 10 ³	250 × 10 ³	50 × 10 ³	100 × 10 ³	150 × 10 ³	200 × 10 ³	250 × 10 ³
1	0	---	8.40	17.00	27.00	37.00	47.70	0.168 × 10 ⁻³	0.170 × 10 ⁻³	0.180 × 10 ⁻³	0.185 × 10 ⁻³	0.191 × 10 ⁻³
2	.8	0	9.60	19.45	30.15	41.10	52.30	.192	.195	.201	.206	.209
3	1.6	0	8.00	16.50	25.90	36.00	47.00	.160	.165	.173	.180	.188
4	1.6	90	9.20	18.40	28.00	37.85	48.00	.184	.184	.187	.189	.192
5	1.6	180	7.55	16.20	25.60	36.40	48.40	.151	.162	.171	.182	.194
6	1.6	270	---	---	---	---	---	---	---	---	---	---
7	3.2	0	7.00	15.00	23.70	33.10	43.10	.140	.150	.158	.166	.172
8	3.2	45	7.90	15.60	24.30	33.40	43.10	.158	.156	.162	.167	.172
9	3.2	135	7.00	14.70	23.30	32.60	43.00	.140	.147	.155	.163	.172
10	3.2	180	7.00	14.70	23.30	32.60	43.00	.140	.147	.155	.163	.172
11	3.2	225	6.10	13.40	22.00	31.30	41.60	.122	.134	.147	.157	.166
12	3.2	315	8.50	16.50	25.00	34.10	43.90	.170	.165	.167	.171	.176
13	4.8	0	8.10	15.10	22.60	30.30	37.80	.162	.151	.151	.151	.151
14	6.4	0	6.20	11.10	16.80	22.50	28.20	.124	.111	.112	.113	.113
15	6.4	90	6.80	12.10	17.80	23.50	28.80	.136	.121	.119	.118	.115
16	9.6	0	6.40	7.00	9.50	12.80	16.00	.128	.070	.063	.064	.064
17	9.6	45	6.00	6.60	9.00	12.00	15.00	.120	.066	.060	.060	.060
18	12.8	0	4.00	5.00	6.00	6.70	8.40	.080	.050	.040	.034	.034
19	12.8	90	4.00	5.00	6.00	6.20	8.40	.080	.050	.040	.031	.034
20	16	45	.30	1.90	4.27	6.05	6.45	.006	.019	.028	.030	.026
21	19.2	0	---	.47	1.50	2.88	4.15	---	.005	.010	.014	.017
22	19.2	90	.25	.88	1.82	2.98	4.15	.005	.009	.012	.015	.017
23	22.4	45	.27	.57	.67	1.18	1.68	.005	.006	.004	.006	.007
24	25.6	0	.72	.80	.70	.64	.64	.014	.008	.005	.003	.003
25	25.1	90	.52	.80	.94	.90	.87	.010	.008	.006	.004	.003
26	28.8	45	.88	.70	.83	.85	.80	.018	.007	.006	.004	.003
27	32.0	0	.50	.52	.70	.75	.80	.010	.005	.005	.004	.003
28	35.2	45	.50	.70	.83	.85	.90	.010	.007	.006	.004	.004

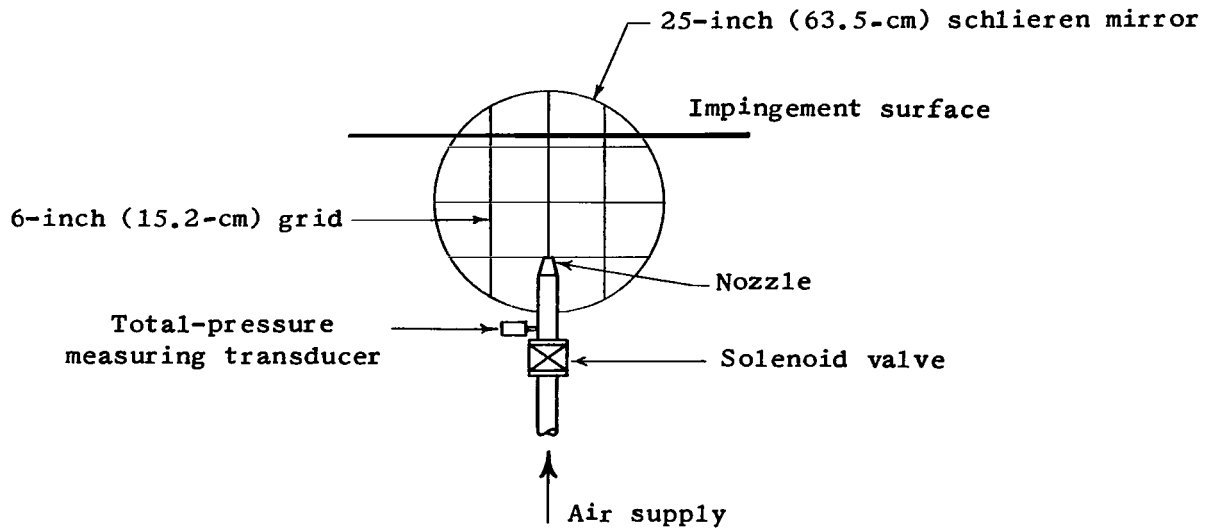
(d) $x/d_j = 40$

Orifice	r/d _j	ψ, deg	P _s /P _∞ for values of P _t /P _∞ of -					P _s /P _t for values of P _t /P _∞ of -				
			①	②	③	④	⑤	⑥	⑦	⑧	⑨	⑩
			50 × 10 ³	100 × 10 ³	150 × 10 ³	200 × 10 ³	250 × 10 ³	50 × 10 ³	100 × 10 ³	150 × 10 ³	200 × 10 ³	250 × 10 ³
1	0	---	2.60	4.00	5.77	7.82	9.98	0.052 × 10 ⁻³	0.040 × 10 ⁻³	0.038 × 10 ⁻³	0.039 × 10 ⁻³	0.040 × 10 ⁻³
2	.8	0	3.17	5.15	7.40	9.67	11.93	.063	.052	.048	.048	.048
3	1.6	0	3.15	5.05	7.10	9.12	11.16	.063	.051	.047	.046	.045
4	1.6	90	2.98	4.88	7.10	9.12	11.16	.060	.049	.047	.046	.045
5	1.6	180	3.11	4.90	6.92	8.93	10.96	.062	.049	.046	.045	.044
6	1.6	270	3.15	4.97	6.92	8.93	10.96	.063	.050	.046	.045	.044
7	3.2	0	2.76	4.52	6.60	8.70	10.80	.055	.045	.044	.044	.044
8	3.2	45	2.60	4.67	7.17	9.58	12.03	.052	.047	.048	.048	.048
9	3.2	135	2.98	4.61	6.40	8.20	10.00	.060	.046	.043	.041	.040
10	3.2	180	1.53	3.26	5.50	7.70	9.92	.031	.033	.037	.039	.040
11	3.2	225	3.26	5.30	7.56	9.70	12.08	.065	.053	.050	.049	.048
12	3.2	315	2.68	4.72	7.17	9.58	12.03	.054	.047	.048	.048	.048
13	4.8	0	2.96	4.47	6.26	7.77	9.42	.059	.045	.042	.039	.038
14	6.4	0	3.13	4.83	6.75	8.68	10.60	.063	.048	.045	.043	.042
15	6.4	90	3.21	4.67	6.39	8.12	9.85	.064	.047	.043	.041	.039
16	9.6	0	3.18	4.36	5.86	7.38	8.91	.064	.044	.039	.037	.036
17	9.6	45	2.62	3.82	5.53	7.26	9.00	.052	.038	.037	.036	.036
18	12.8	0	5.90	4.24	5.20	6.30	7.40	.118	.042	.035	.032	.030
19	12.8	90	5.90	3.66	4.67	5.97	7.27	.118	.037	.031	.030	.029
20	16	45	3.32	5.90	6.69	7.35	8.01	.066	.059	.045	.037	.032
21	19.2	0	.60	4.22	5.80	6.35	7.10	.012	.042	.039	.032	.028
22	19.2	90	1.00	4.22	5.80	6.70	7.65	.020	.042	.039	.034	.031
23	22.4	45	.36	1.90	3.88	5.88	7.90	.007	.019	.026	.029	.032
24	25.6	0	.50	.93	2.00	3.22	4.48	.010	.009	.013	.016	.018
25	25.6	90	.50	.82	1.83	3.01	4.19	.010	.008	.009	.015	.017
26	28.8	45	.92	.61	1.13	1.69	2.24	.018	.006	.008	.008	.009
27	32.0	0	1.08	.77	.80	1.00	1.20	.022	.008	.005	.005	.005
28	35.2	45	.82	.77	.80	1.00	1.20	.016	.008	.005	.005	.005

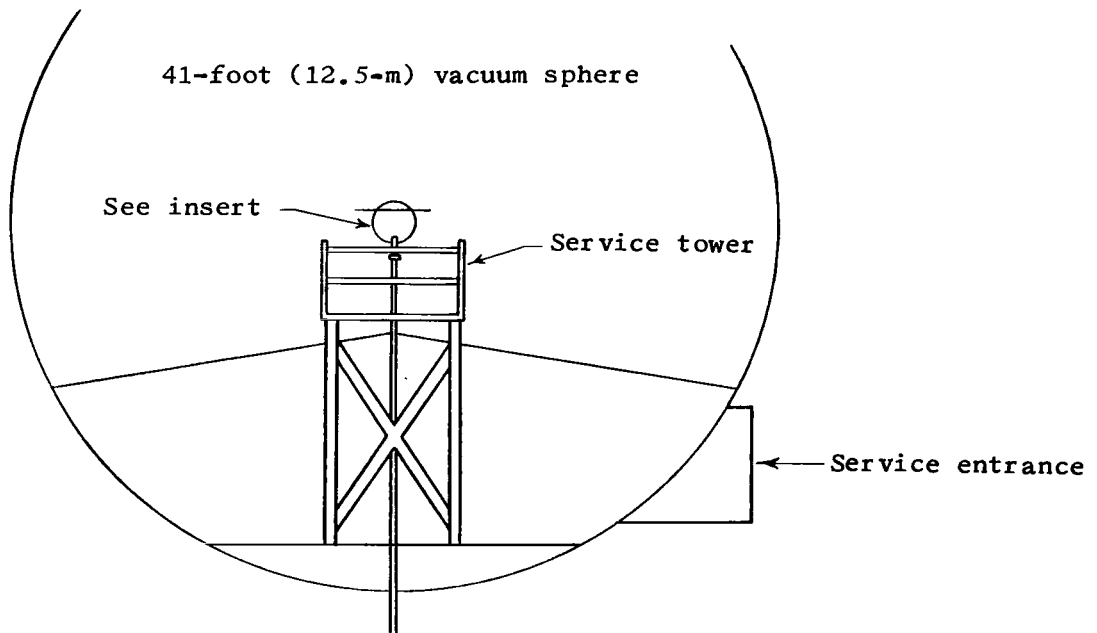
TABLE II - SURFACE-PRESSURE-DATA RESULTS OF $M_j = 5.0$ NOZZLE EXHAUST PLUME
IMPINGING UPON A PERPENDICULAR FLAT SURFACE - Concluded

(e) $x/d_j = 80$

Orifice	r/d_j	ψ , deg	①	②	③	④	⑤	⑥	⑦	⑧	⑨	⑩
			P_B/P_∞ for values of P_t/P_∞ of -					P_B/P_t for values of P_t/P_∞ of -				
			50×10^3	100×10^3	150×10^3	200×10^3	250×10^3	50×10^3	100×10^3	150×10^3	200×10^3	250×10^3
1	0	---	9.00	1.00	1.00	1.00	1.00	0.180×10^{-3}	0.010×10^{-3}	0.007×10^{-3}	0.005×10^{-3}	0.004×10^{-3}
2	.8	0	8.55	1.60	1.94	2.28	2.62	.171	.016	.013	.011	.010
3	1.6	0	8.80	2.00	2.40	2.88	3.32	.176	.020	.016	.014	.013
4	1.6	90	9.20	1.90	2.35	2.80	3.28	.184	.019	.016	.014	.013
5	1.6	180	8.40	1.98	2.34	2.70	3.06	.168	.020	.016	.014	.012
6	1.6	270	9.25	2.05	2.48	2.90	3.36	.185	.021	.017	.015	.013
7	3.2	0	8.38	1.40	1.90	2.45	3.00	.168	.014	.013	.012	.012
8	3.2	45	7.65	1.61	2.26	2.94	3.61	.153	.016	.015	.015	.014
9	3.2	135	8.90	2.16	2.60	3.05	3.48	.178	.022	.017	.015	.014
10	3.2	180	10.43	1.60	2.63	3.62	4.60	.209	.016	.018	.018	.018
11	3.2	225	7.75	1.91	2.40	2.88	3.35	.155	.019	.016	.014	.013
12	3.2	315	8.25	1.55	2.18	2.82	3.45	.165	.016	.015	.014	.014
13	4.8	0	8.27	2.00	2.45	2.98	3.52	.165	.020	.016	.015	.014
14	6.4	0	7.25	2.05	2.77	3.25	3.61	.145	.021	.018	.016	.014
15	6.4	90	6.90	2.20	2.60	3.15	3.70	.138	.022	.017	.016	.015
16	9.6	0	4.78	1.76	2.42	3.14	3.85	.096	.018	.016	.016	.015
17	9.6	45	3.82	1.50	2.25	2.83	3.40	.076	.015	.015	.014	.014
18	12.8	0	2.55	2.22	2.72	3.25	3.78	.051	.022	.018	.016	.015
19	12.8	90	2.07	1.57	2.23	2.88	3.56	.041	.016	.015	.014	.014
20	16	45	1.27	2.25	2.60	3.15	3.70	.025	.022	.017	.016	.015
21	19.2	0	.30	5.00	2.50	2.60	2.66	.006	.050	.017	.013	.011
22	19.2	90	.80	2.50	3.50	3.30	3.50	.016	.025	.023	.017	.014
23	22.4	45	.40	4.00	4.20	2.92	2.57	.008	.040	.028	.015	.010
24	25.6	0	.60	2.95	4.35	5.70	3.60	.012	.030	.029	.028	.014
25	25.6	90	.60	2.80	5.85	3.76	3.10	.012	.028	.039	.019	.012
26	28.8	45	1.00	2.20	4.45	5.60	4.30	.020	.022	.030	.028	.017
27	32.0	0	.90	.90	2.10	3.80	5.52	.018	.009	.014	.019	.022
28	35.2	45	.90	.90	1.33	2.12	3.10	.018	.009	.009	.011	.012

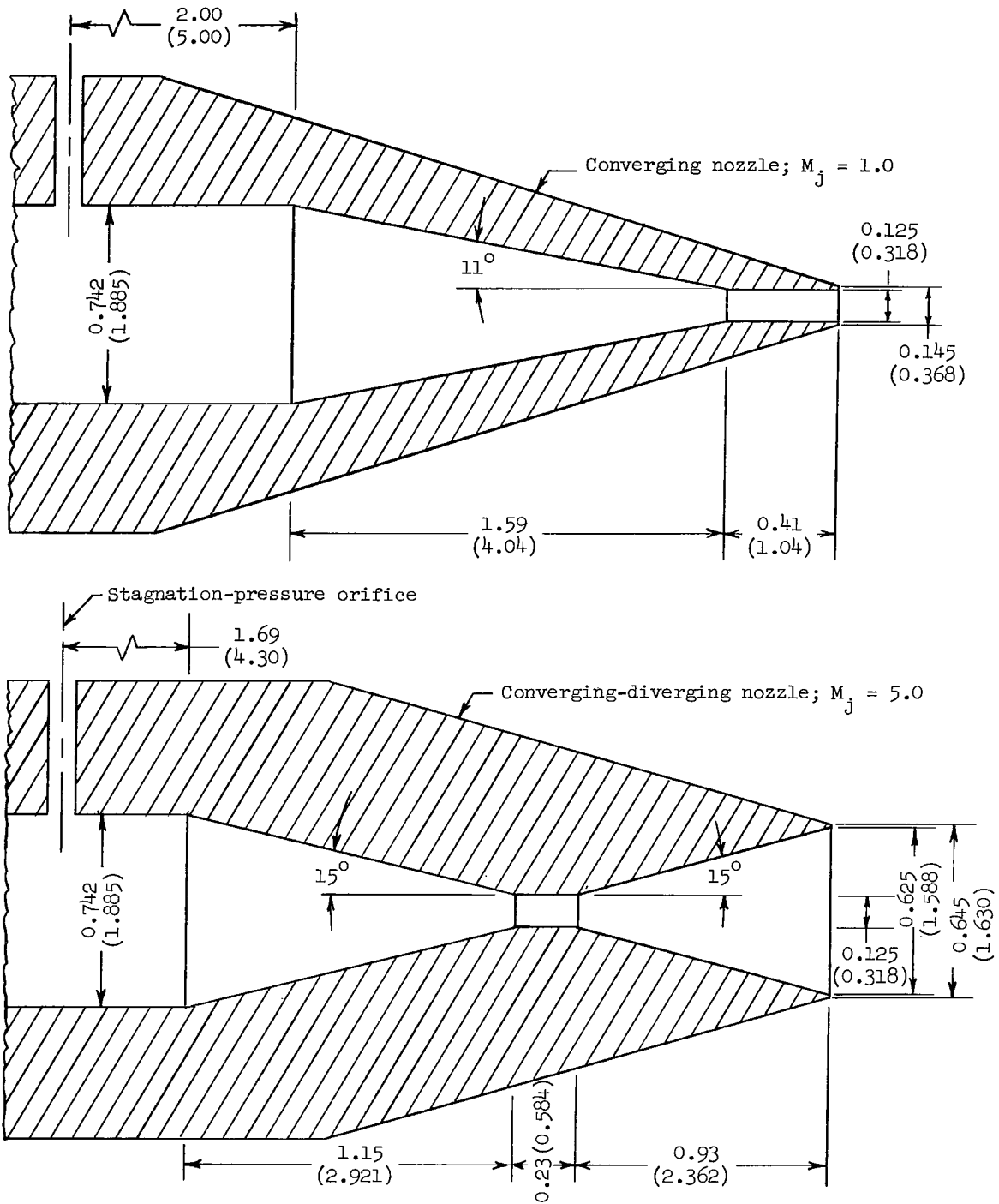


Insert



(a) Overall test setup.

Figure 1- Test facility and nozzles used in impingement investigation.



(b) Test nozzles. All linear dimensions are given in inches and parenthetically in centimeters.

Figure 1- Concluded.

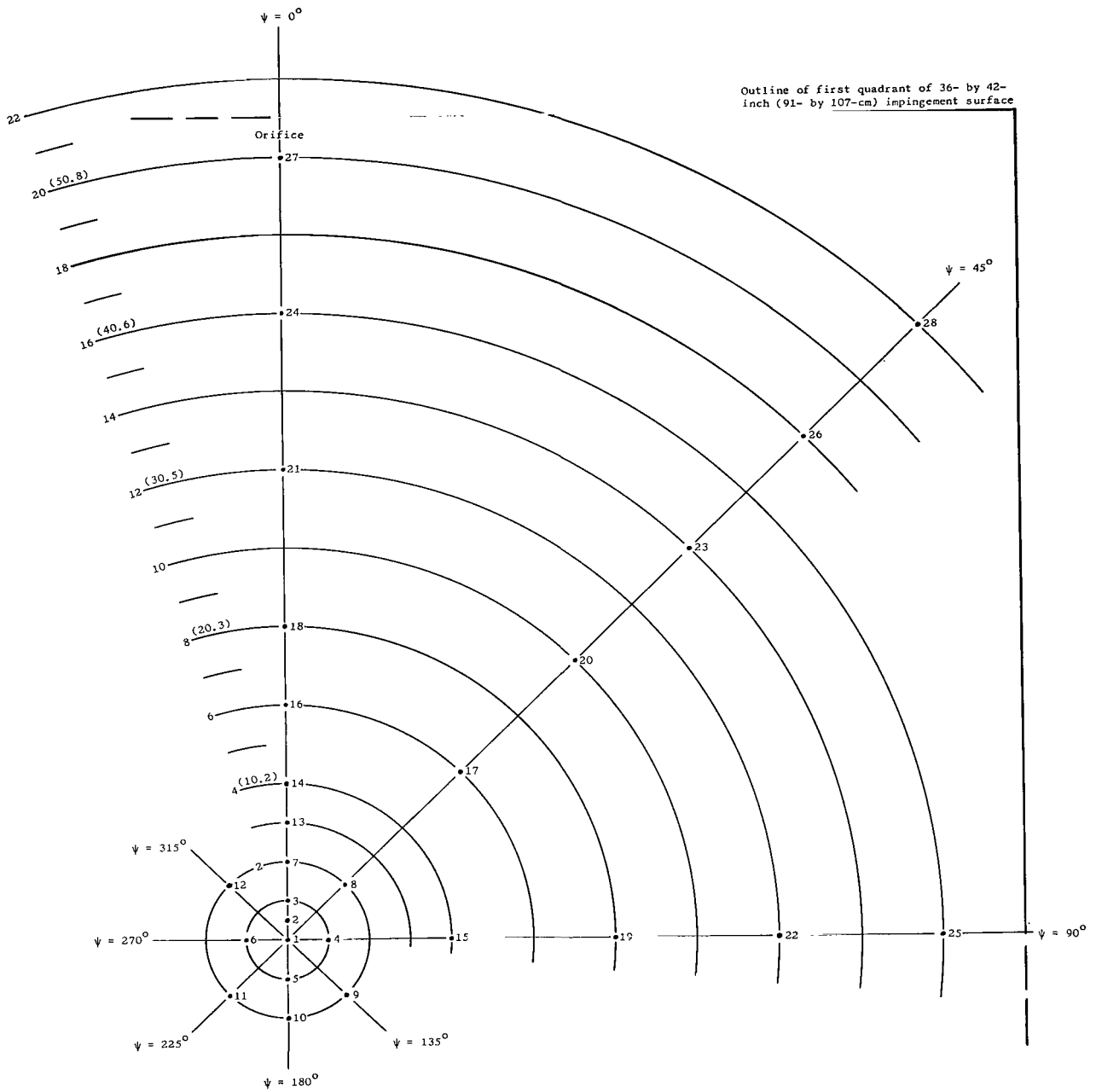
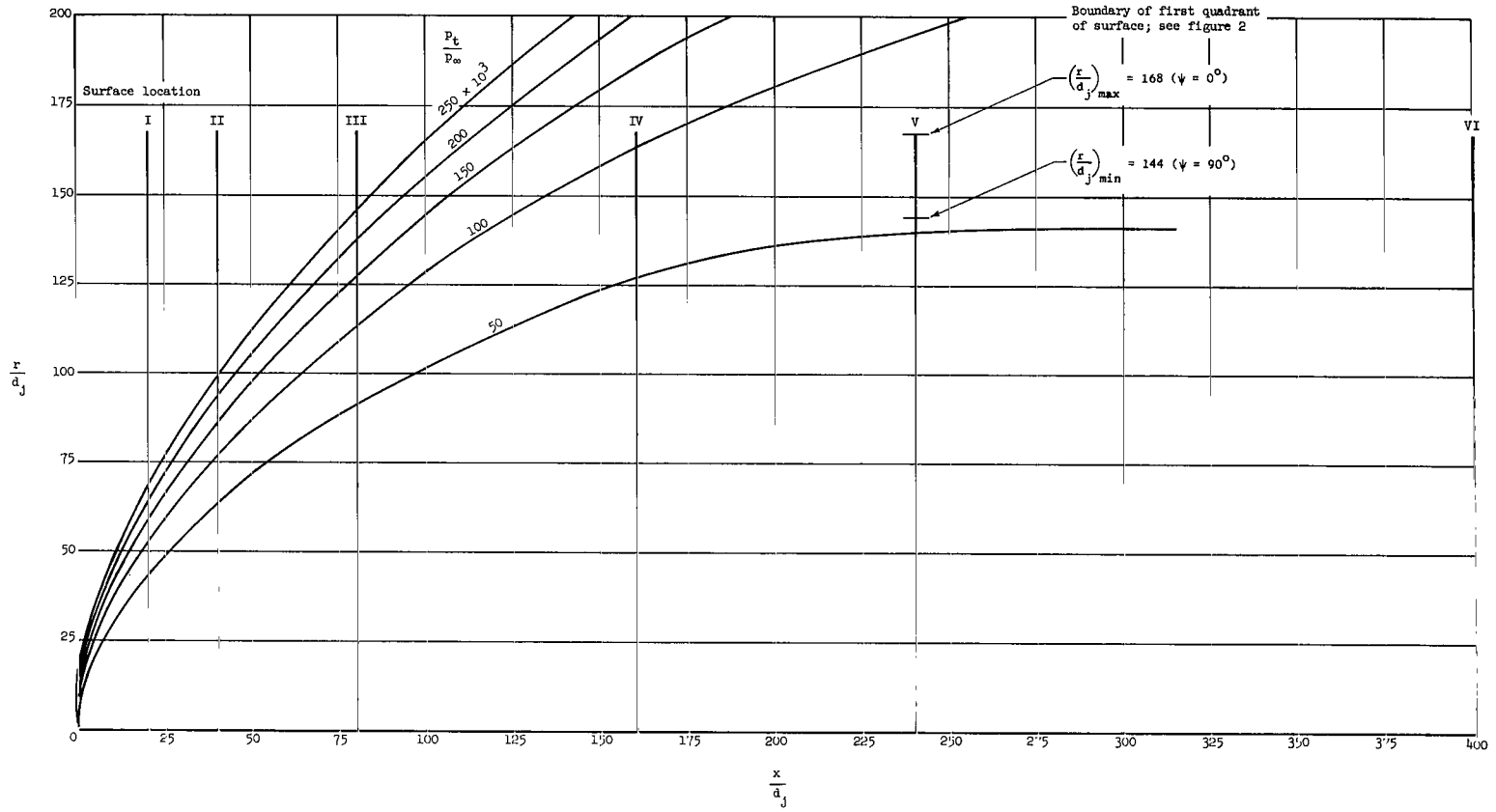
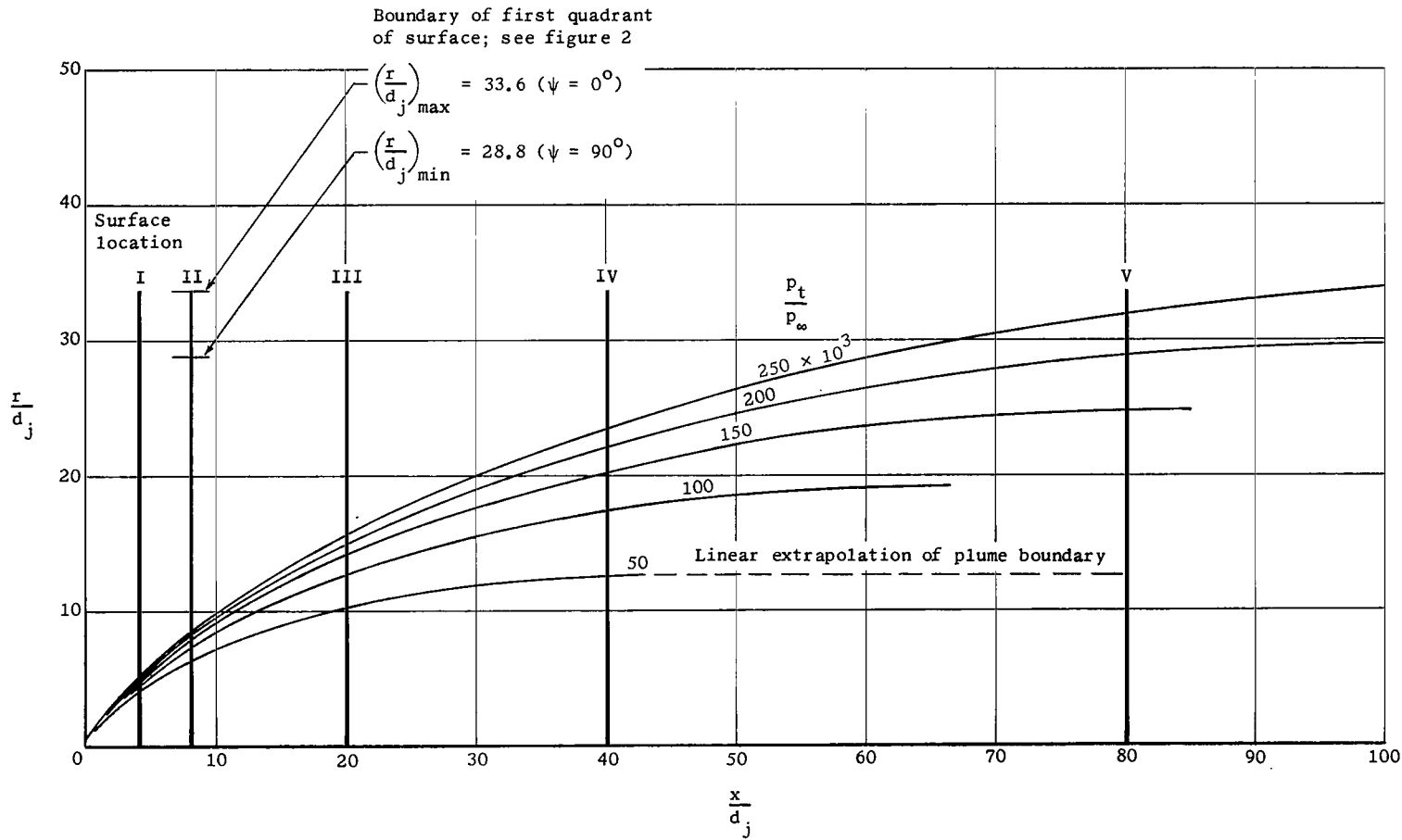


Figure 2.- Static-pressure orifice locations on impingement surface. Linear dimensions are given in inches and parenthetically in centimeters.



(a) $M_j = 1.0; \gamma = 1.4.$

Figure 3.- Correlation of surface positions with nozzle exhaust-plume boundaries. Plume boundary values obtained from theoretical calculations of reference 14.



(b) $M_j = 4.79$; $\theta_n = 26.5^\circ$; $\gamma = 1.4$.

Figure 3.- Concluded.

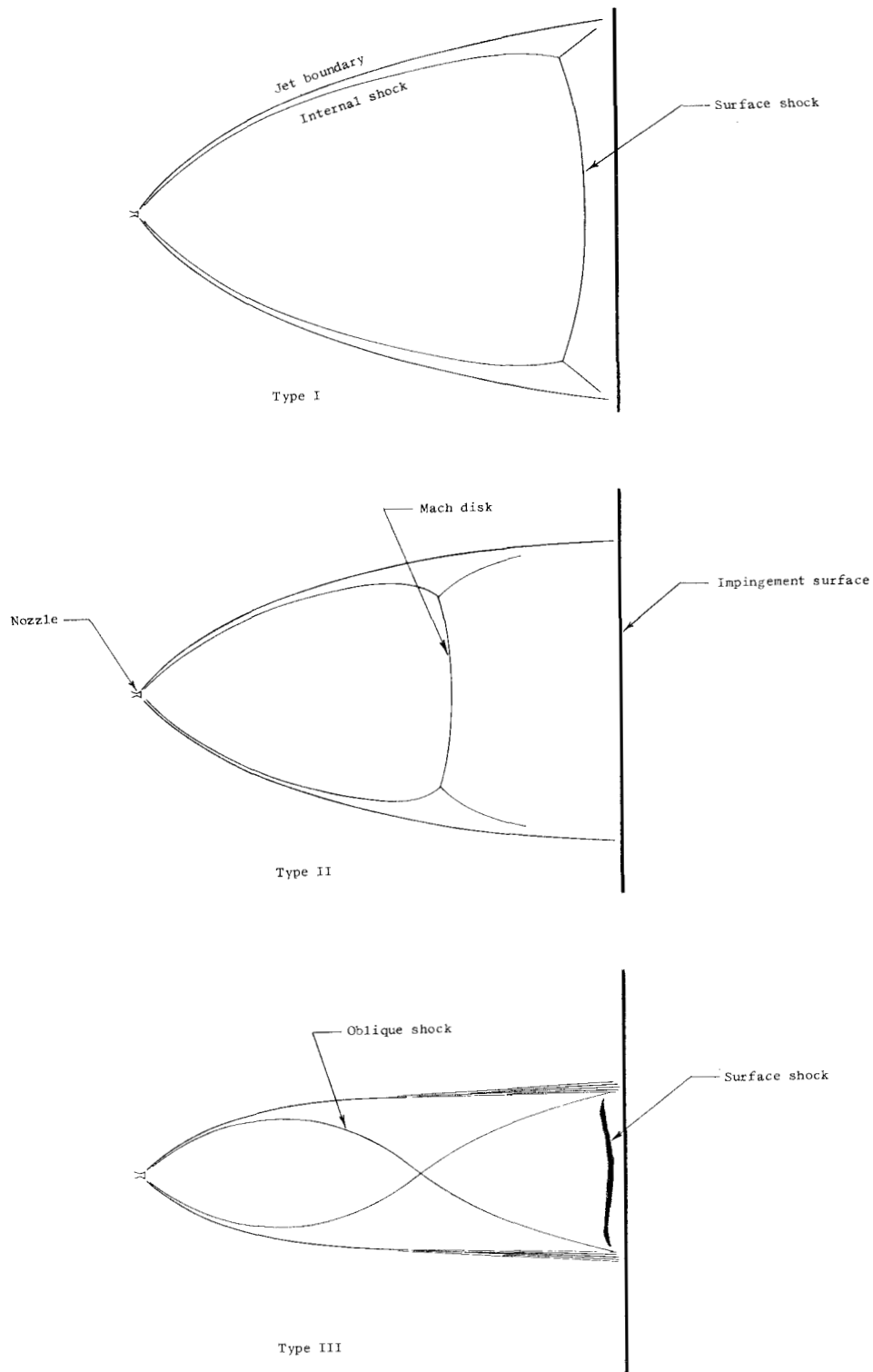
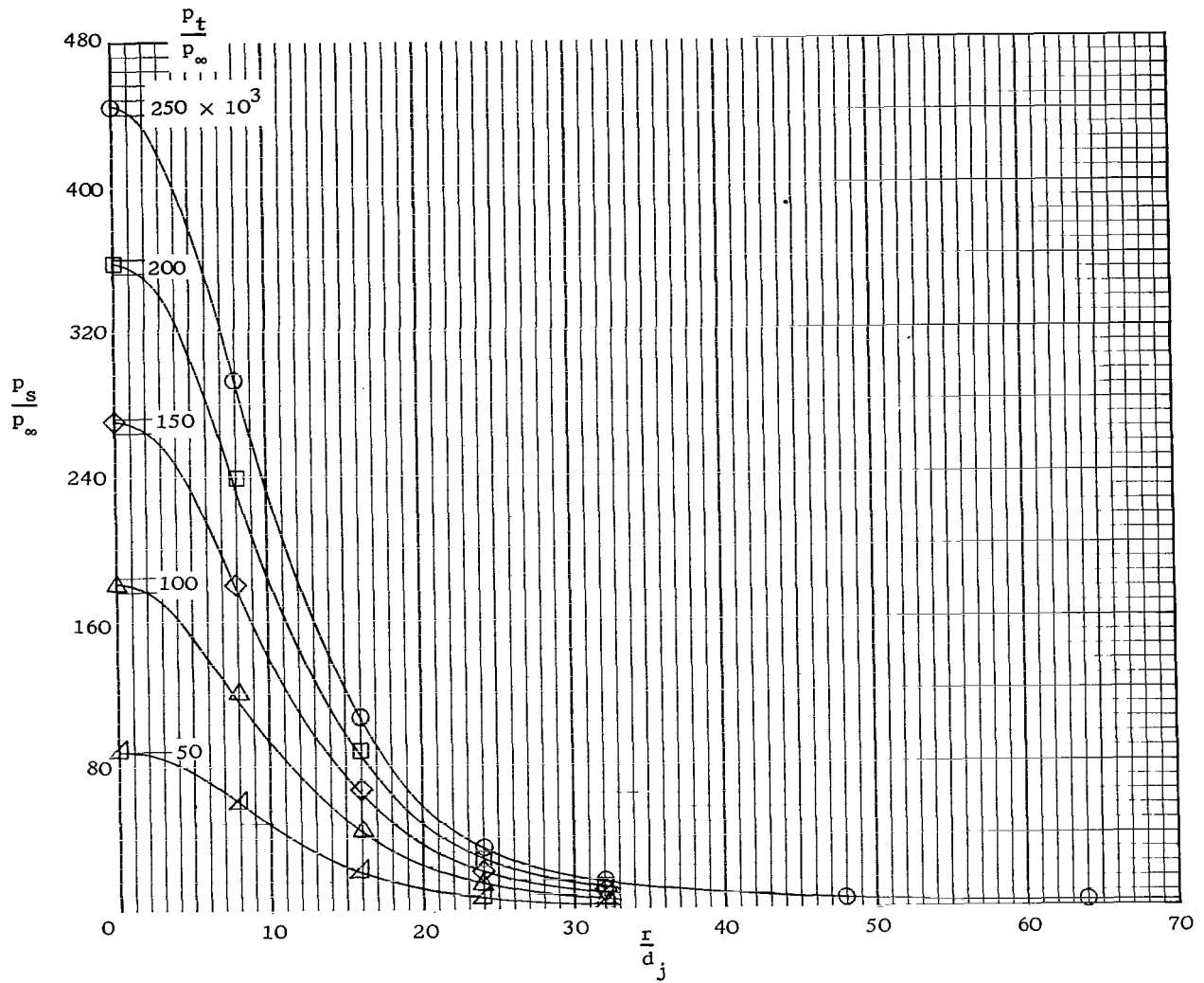
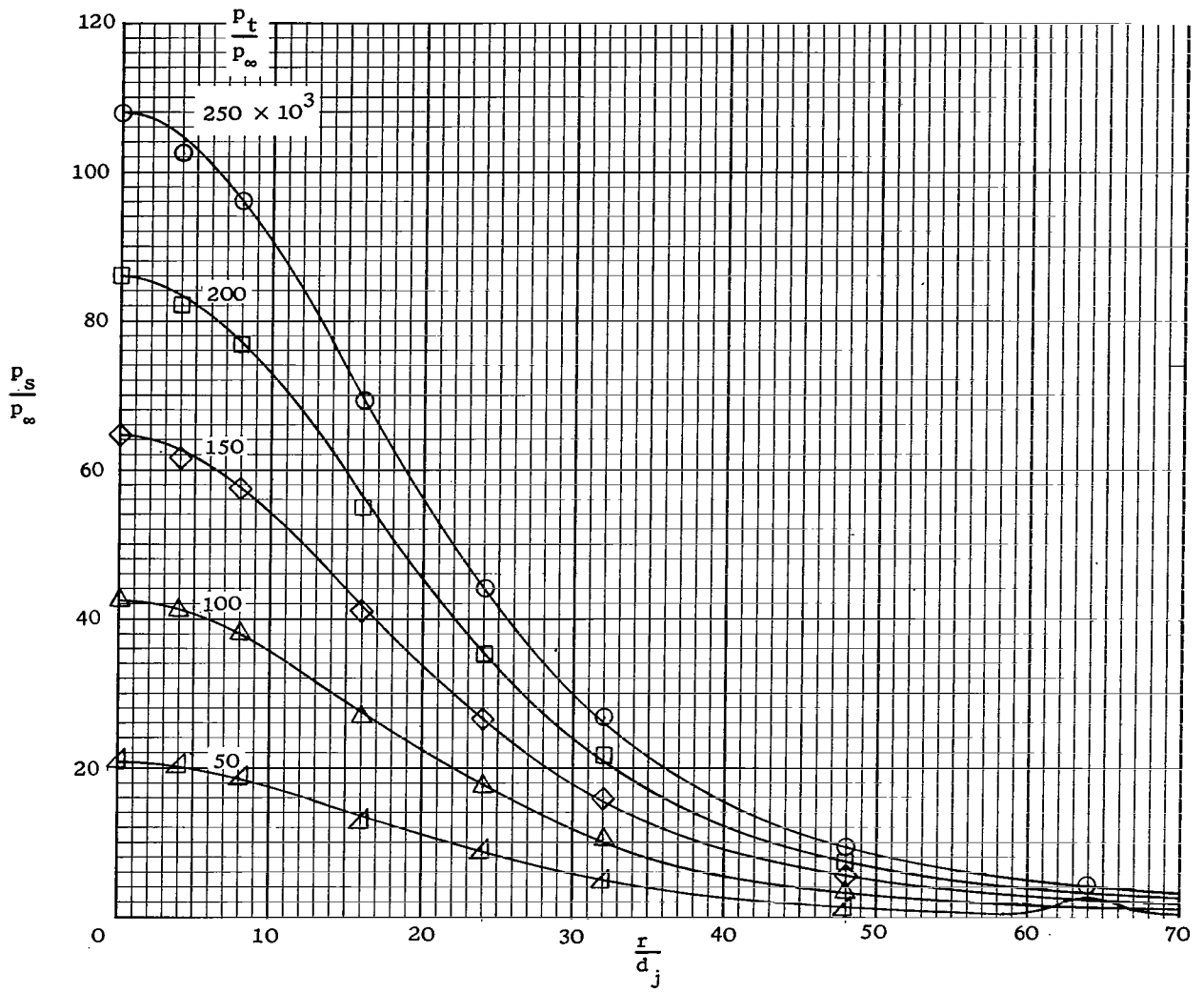


Figure 4.- Sketches of three types of shock formations.



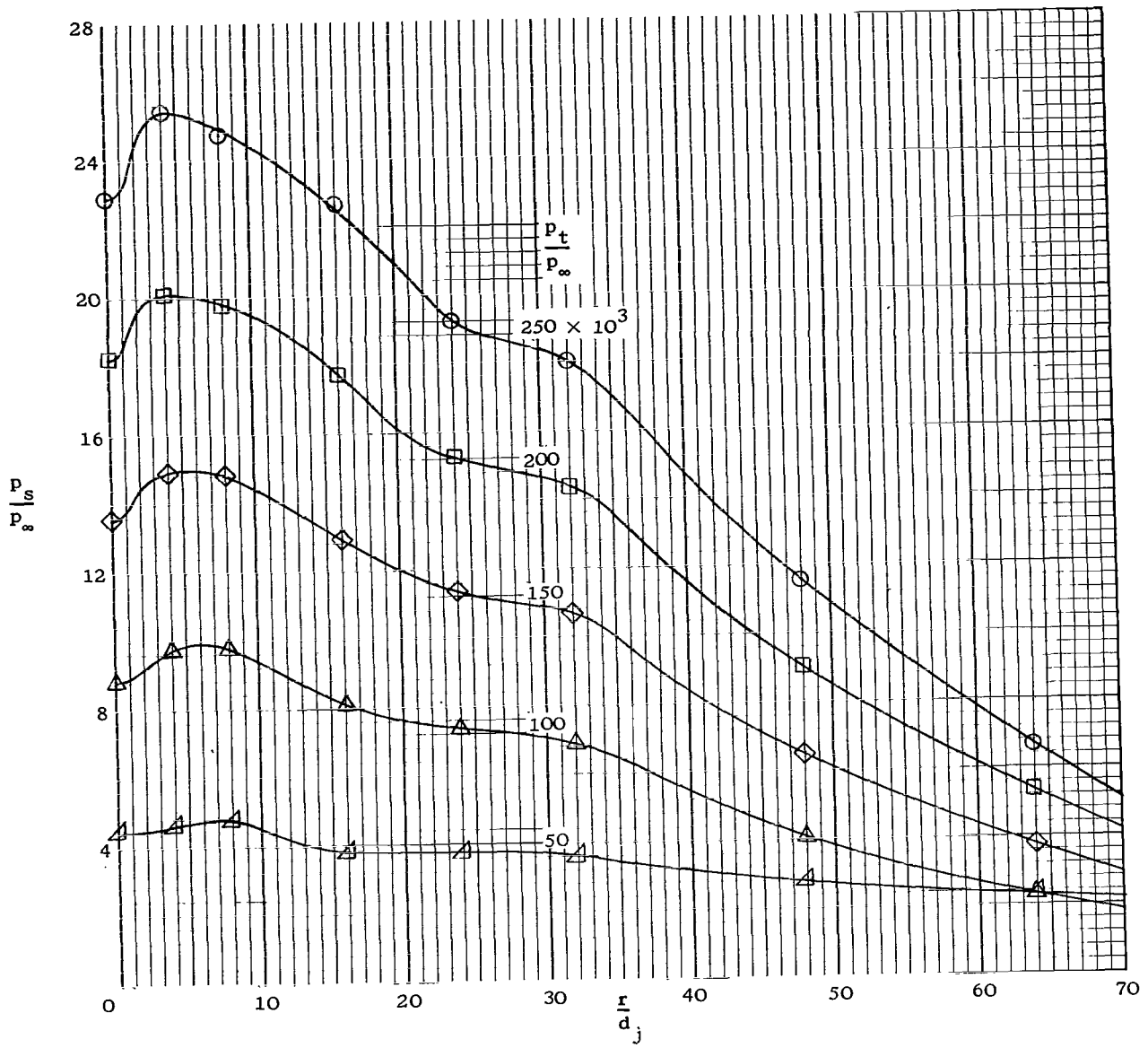
(a) $\frac{x}{d_j} = 20$.

Figure 5.- Distribution of ratio of impingement-surface static pressure to ambient pressure for various ratios of nozzle total pressure to ambient pressure. $M_j = 1.0$; $d_j = 0.125$ in. (0.318 cm); $\psi = 0^\circ$.



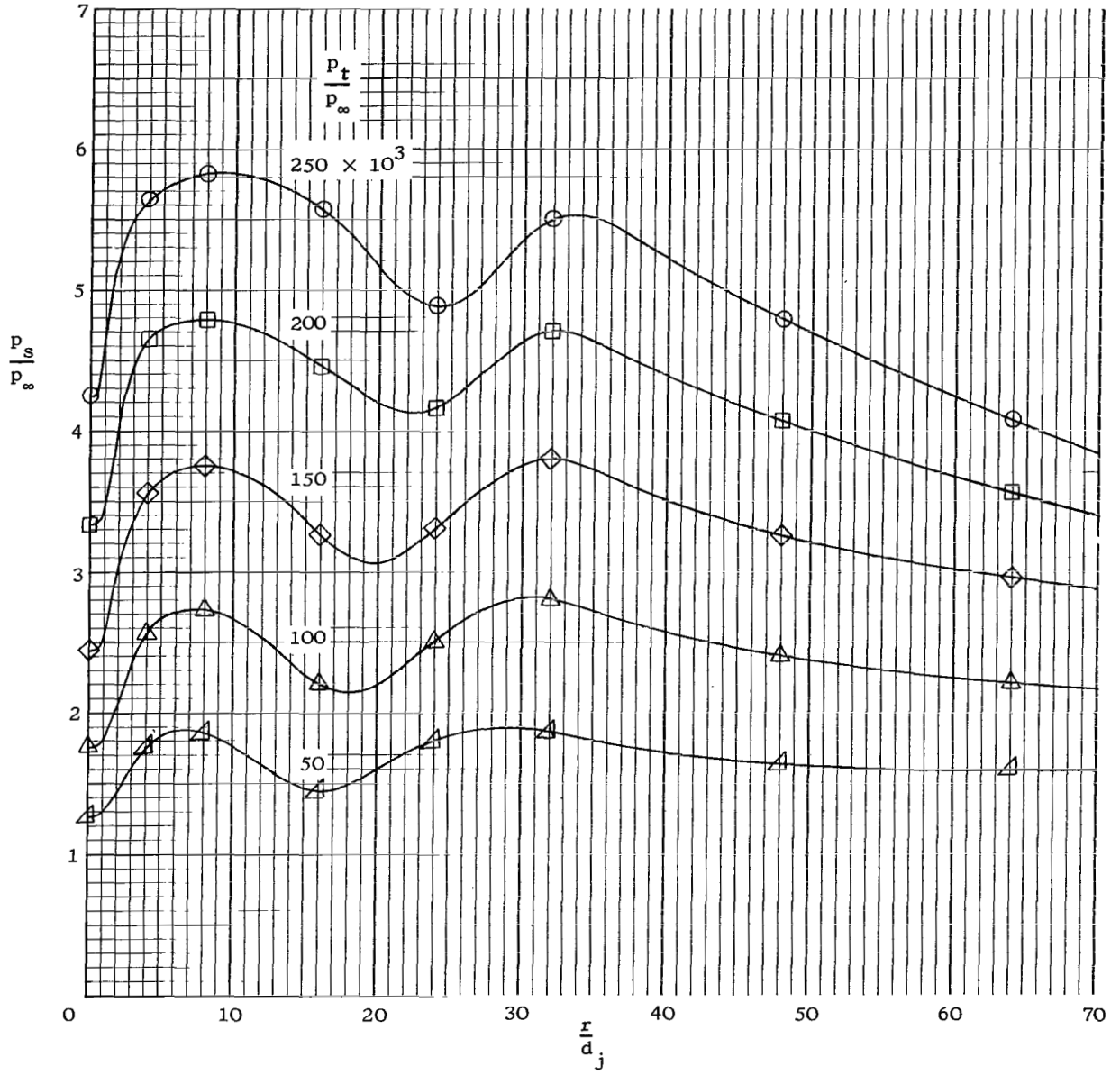
(b) $\frac{x}{d_j} = 40.$

Figure 5.- Continued.



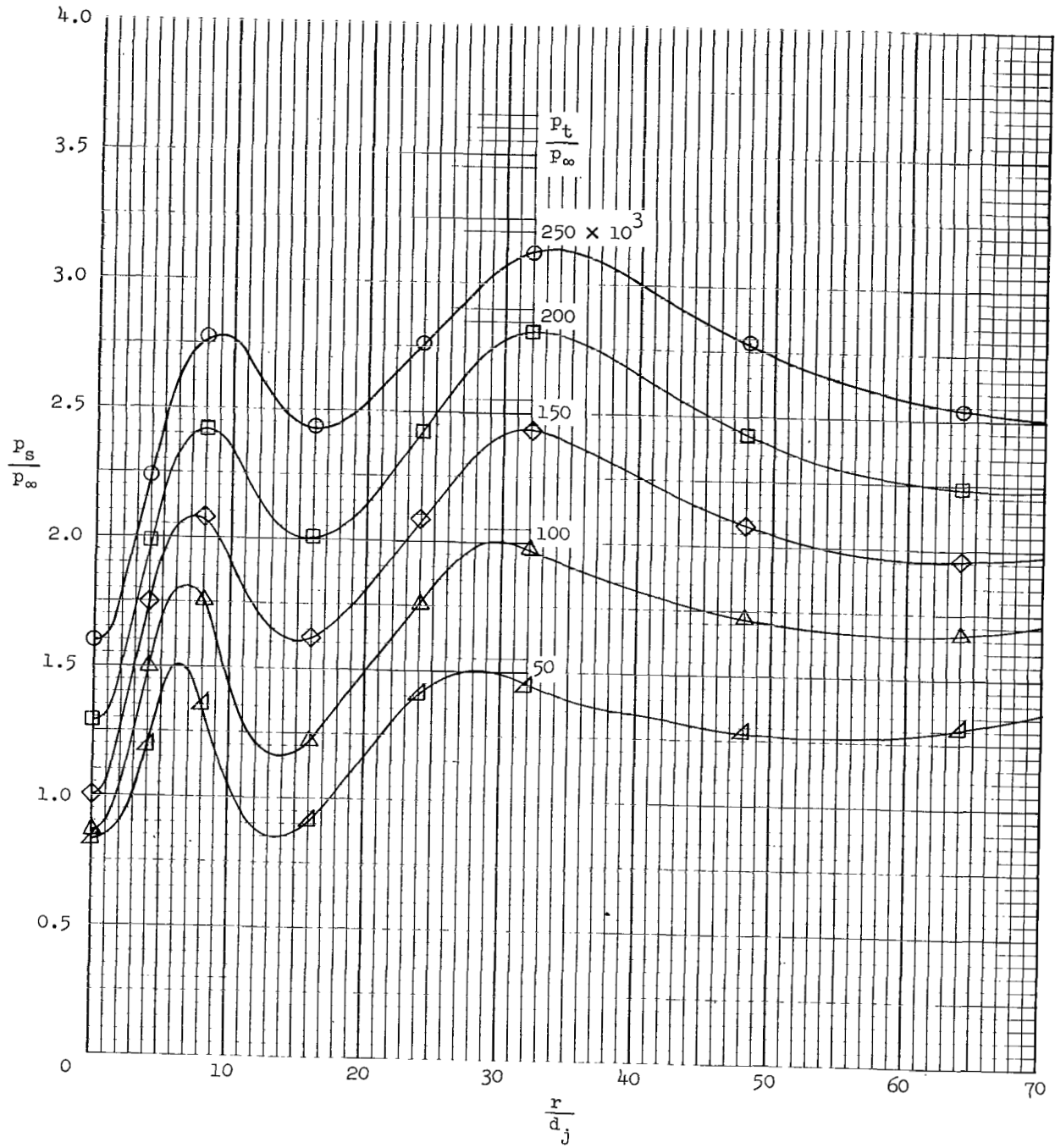
(c) $\frac{x}{d_j} = 80$.

Figure 5.- Continued.



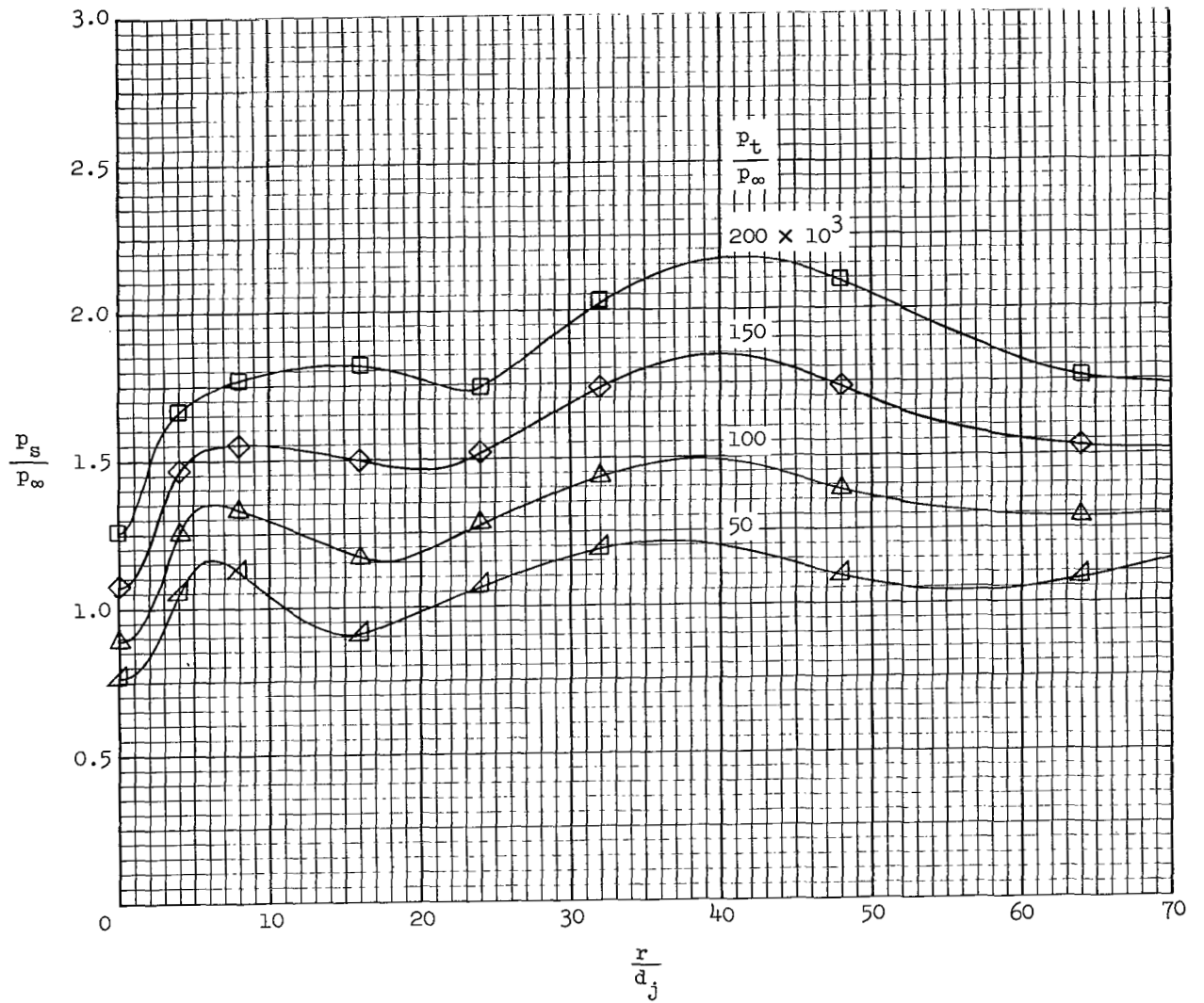
(d) $\frac{x}{d_j} = 160$.

Figure 5.- Continued.



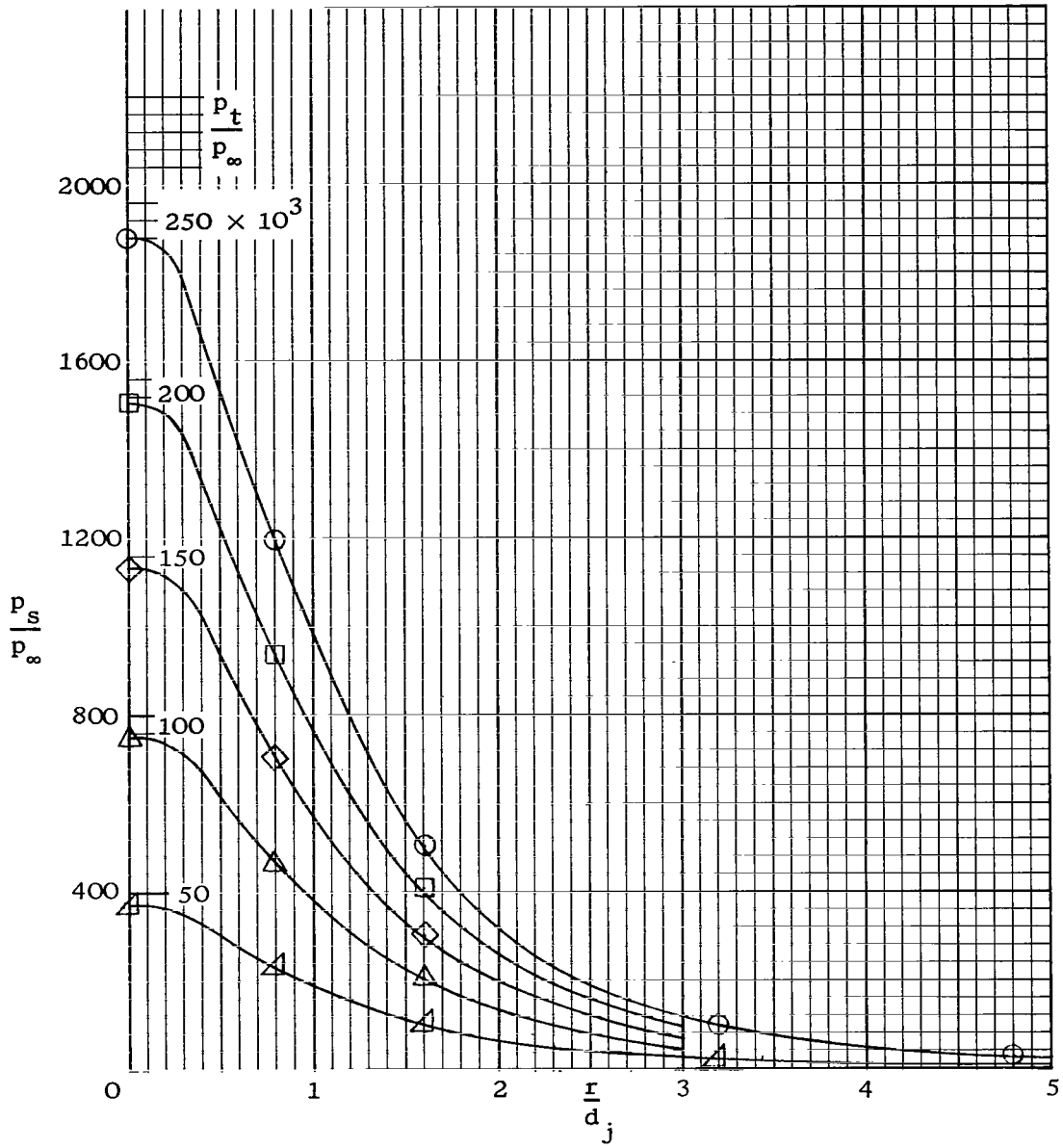
(e) $\frac{x}{d_j} = 240$.

Figure 5.- Continued.



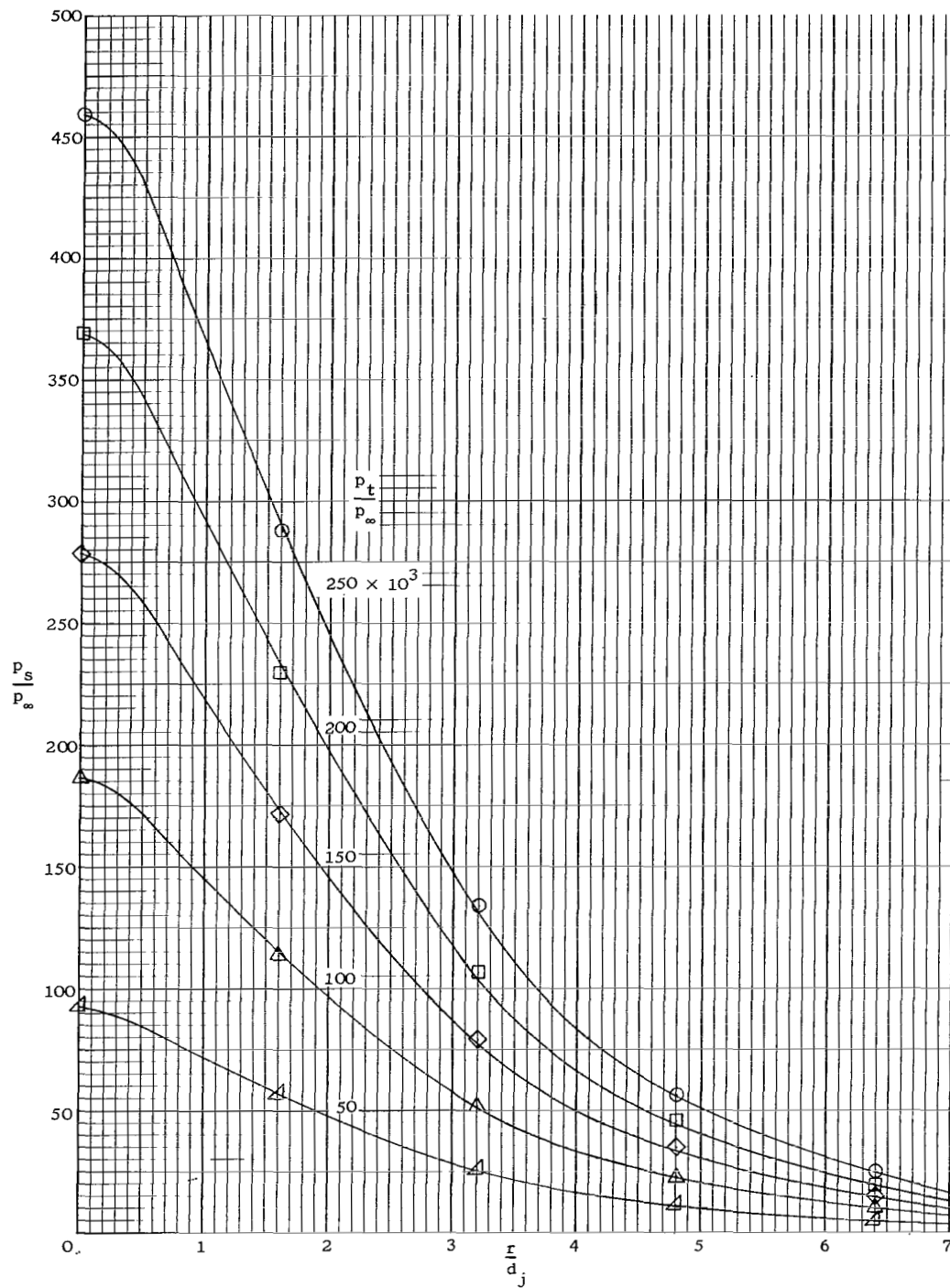
(f) $\frac{x}{d_j} = 400$.

Figure 5.- Concluded.



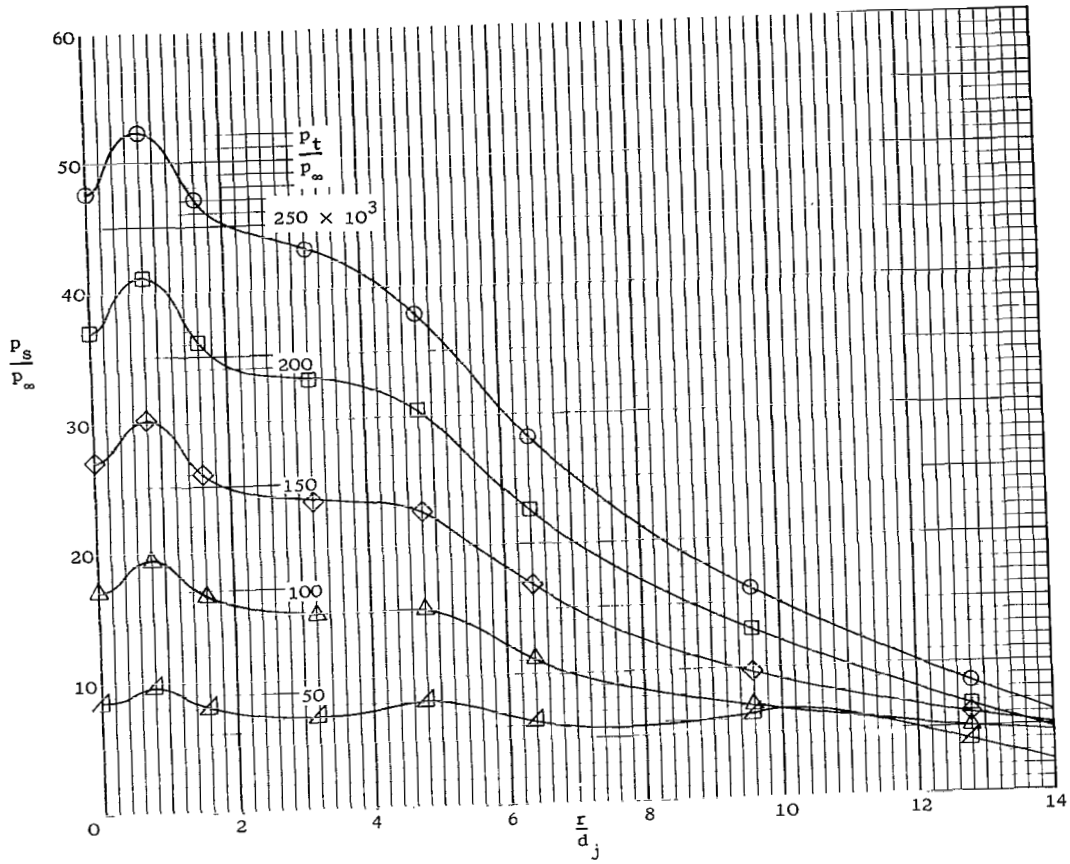
(a) $\frac{x}{d_j} = 4$; $\psi = 0^\circ$.

Figure 6.- Distribution of ratio of impingement-surface static pressure to ambient pressure for various ratios of nozzle total pressure to ambient pressure. $M_j = 5.0$; $d_j = 0.625$ in. (1.588 cm).



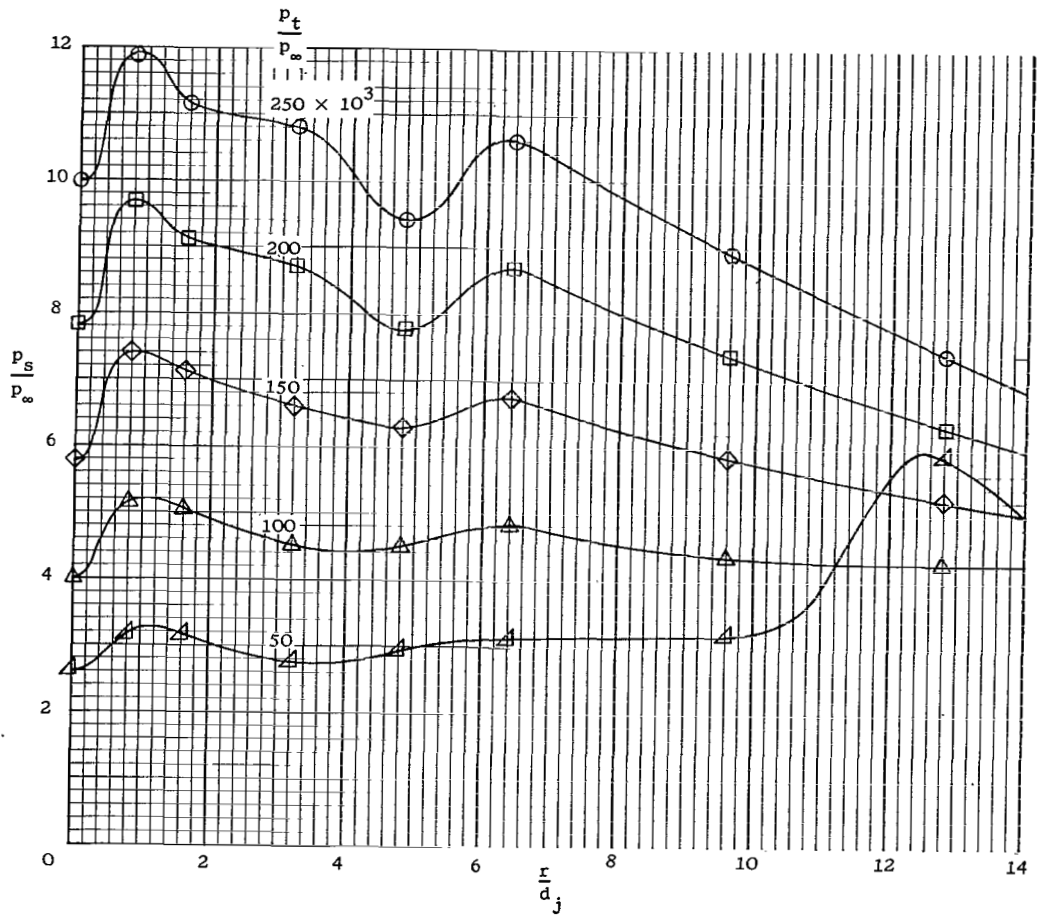
(b) $\frac{\lambda}{d_j} = 8; \psi = 0^\circ.$

Figure 6.- Continued.



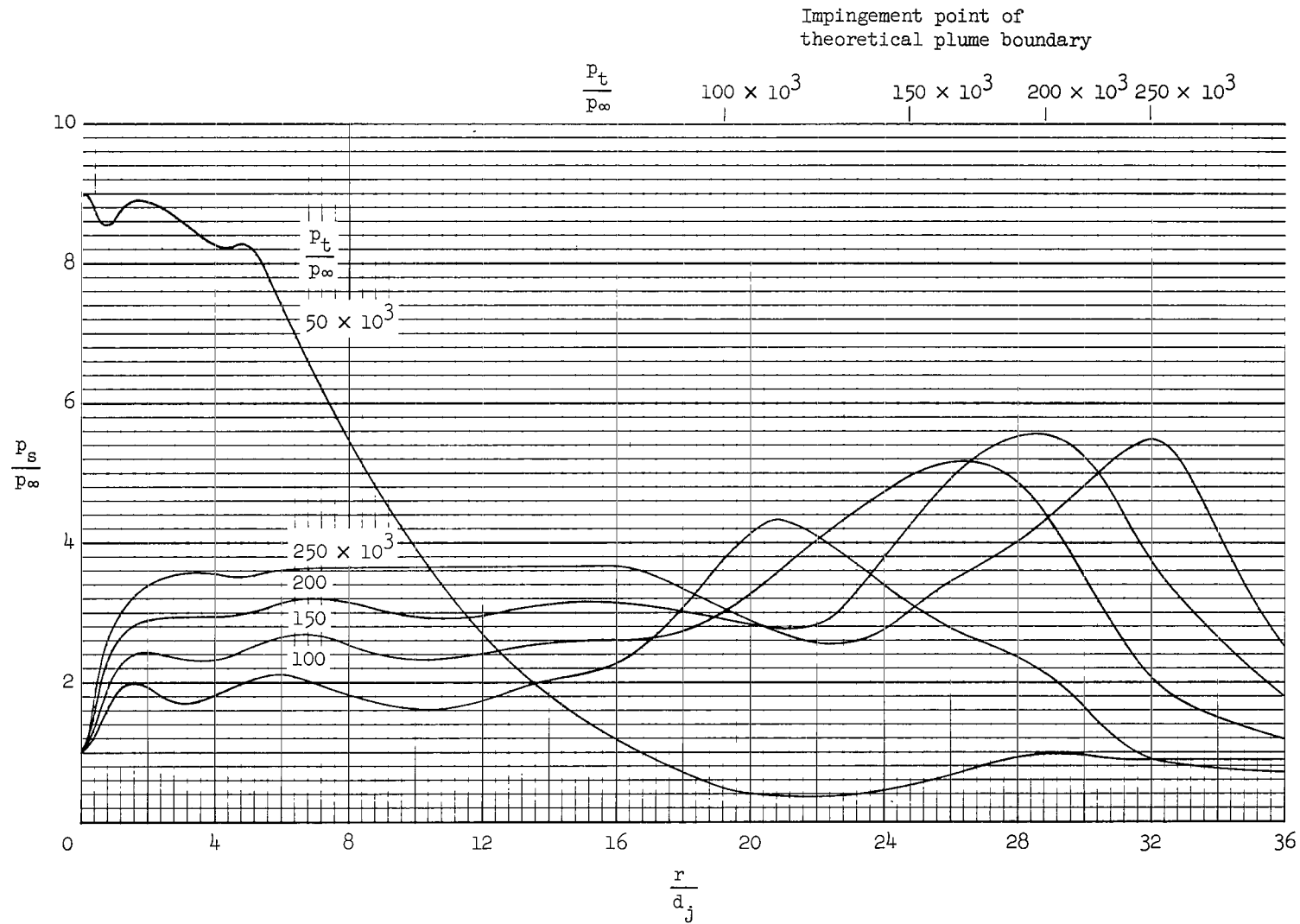
(c) $\frac{x}{d_j} = 20$; $\psi = 0^\circ$.

Figure 6.- Continued.



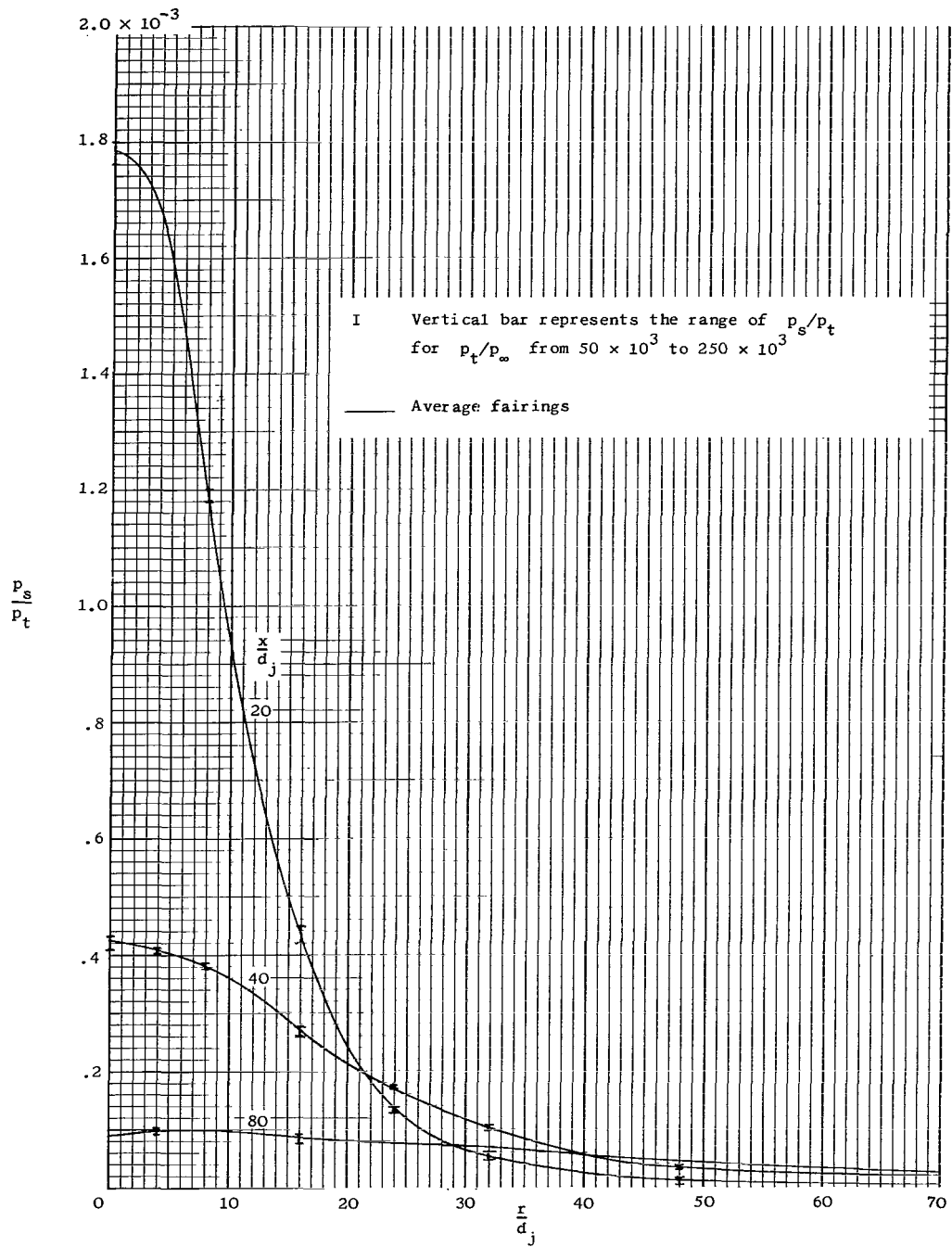
(d) $\frac{x}{d_j} = 40; \psi = 0^\circ.$

Figure 6.- Continued.



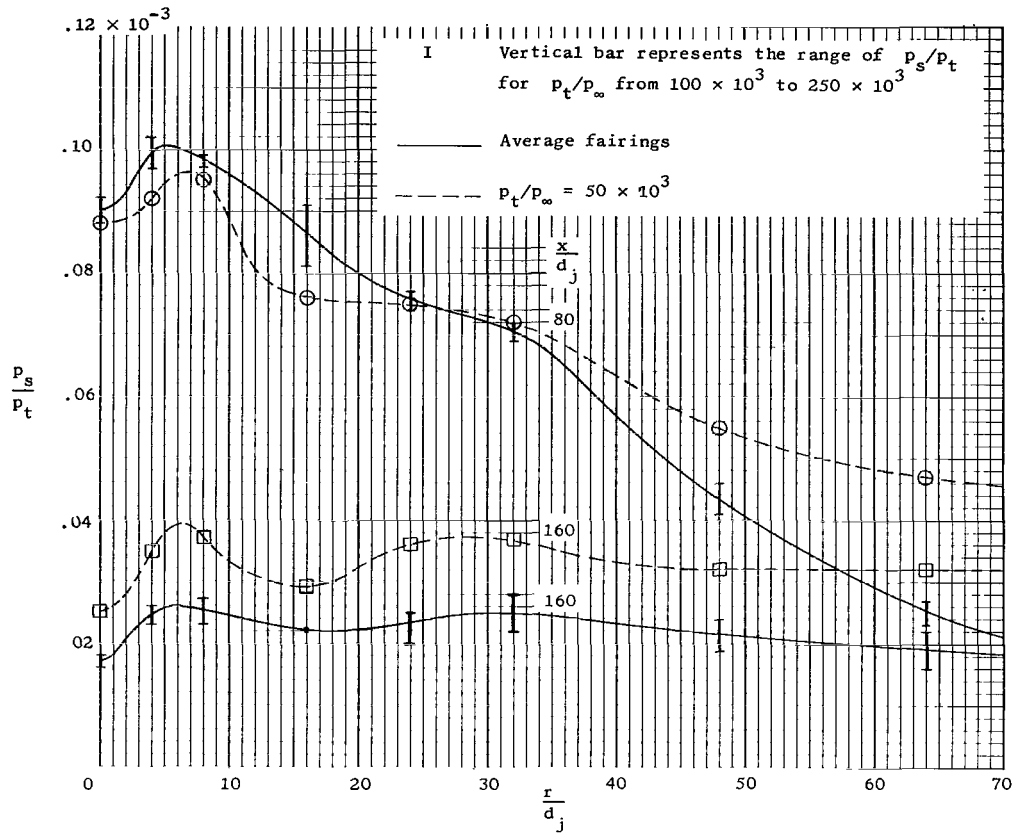
(e) $\frac{x}{d_j} = 80$. (Data have been numerically averaged for each $\frac{r}{d_j}$ value.)

Figure 6.- Concluded.



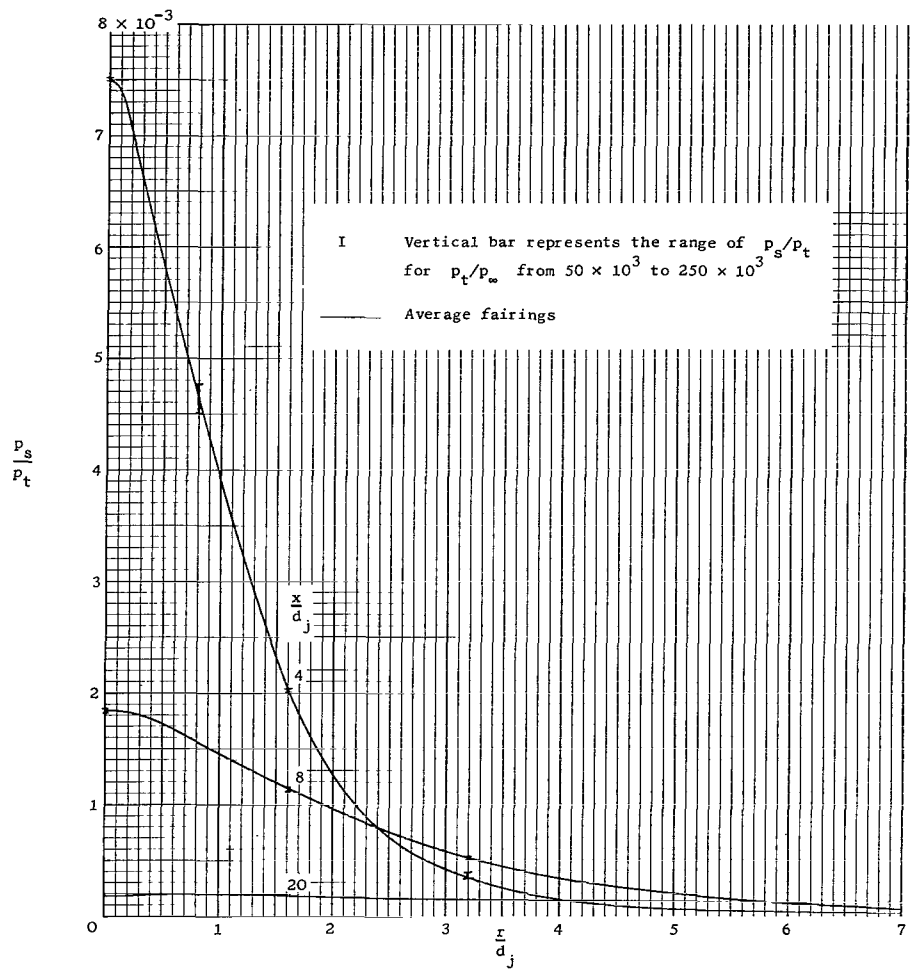
(a) $\frac{x}{d_j} = 20, 40, \text{ and } 80.$

Figure 7.- Distribution of ratio of impingement-surface static pressure to nozzle total pressure for various nozzle-to-surface separation distances $M_j = 1.0$; $\psi = 0^\circ$.



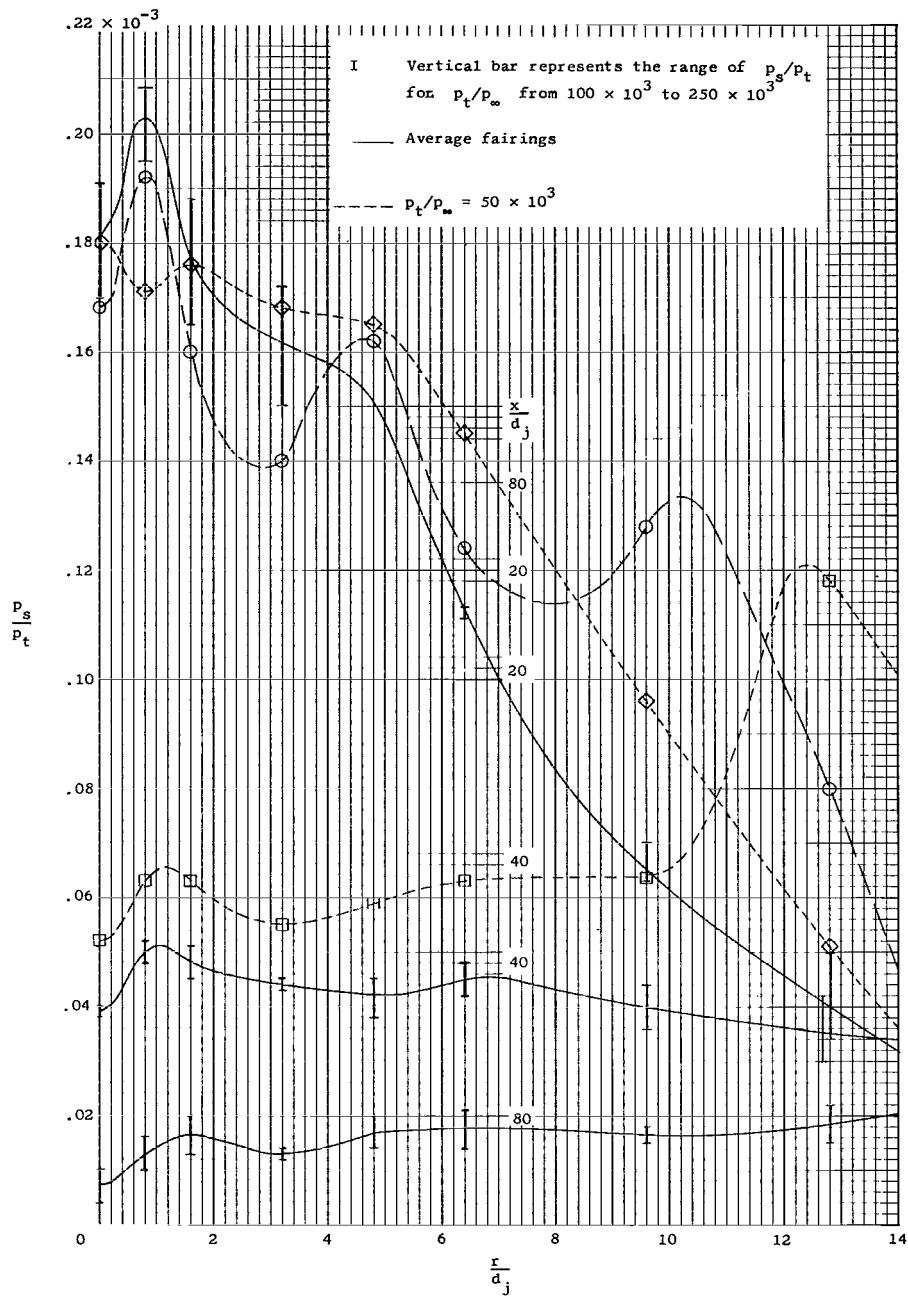
(b) $\frac{x}{d_j} = 80$ and 160 .

Figure 7.- Concluded.



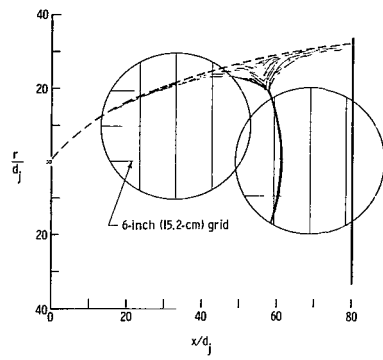
(a) $\frac{x}{d_j} = 4, 8, \text{ and } 20.$

Figure 8.- Distribution of ratio of impingement-surface static pressure to nozzle total pressure for various nozzle-to-surface separation distances. $M_j = 5.0$; $\psi = 0^\circ$.

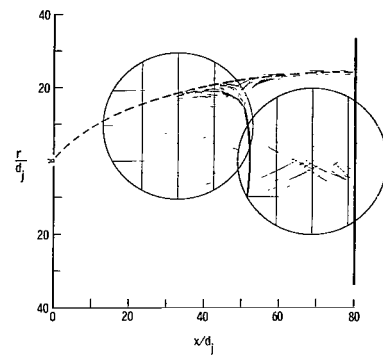


(b) $\frac{x}{d_j} = 20, 40, \text{ and } 80.$

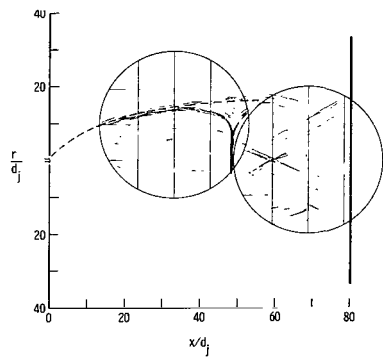
Figure 8.- Concluded.



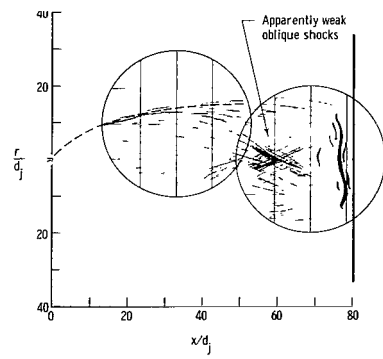
(a) $p_t/p_\infty = 250 \times 10^3$.



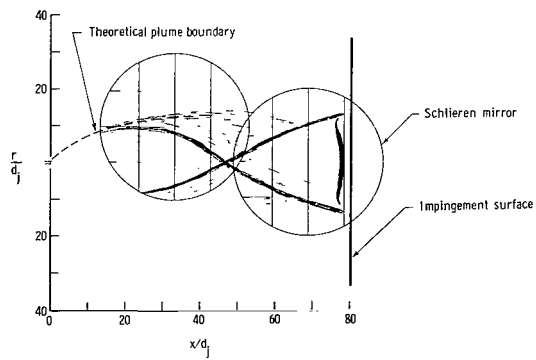
(b) $p_t/p_\infty = 150 \times 10^3$.



(c) $p_t/p_\infty = 81.25 \times 10^3$.



(d) $p_t/p_\infty = 67 \times 10^3$.



(e) $p_t/p_\infty = 50 \times 10^3$.

Figure 9.- Sketches showing shock formations in relation to the impingement surface. $M_j = 5.0$; $x/d_j = 80$. The various shadings in sketches represent what was actually observed in viewing the schlieren movies.

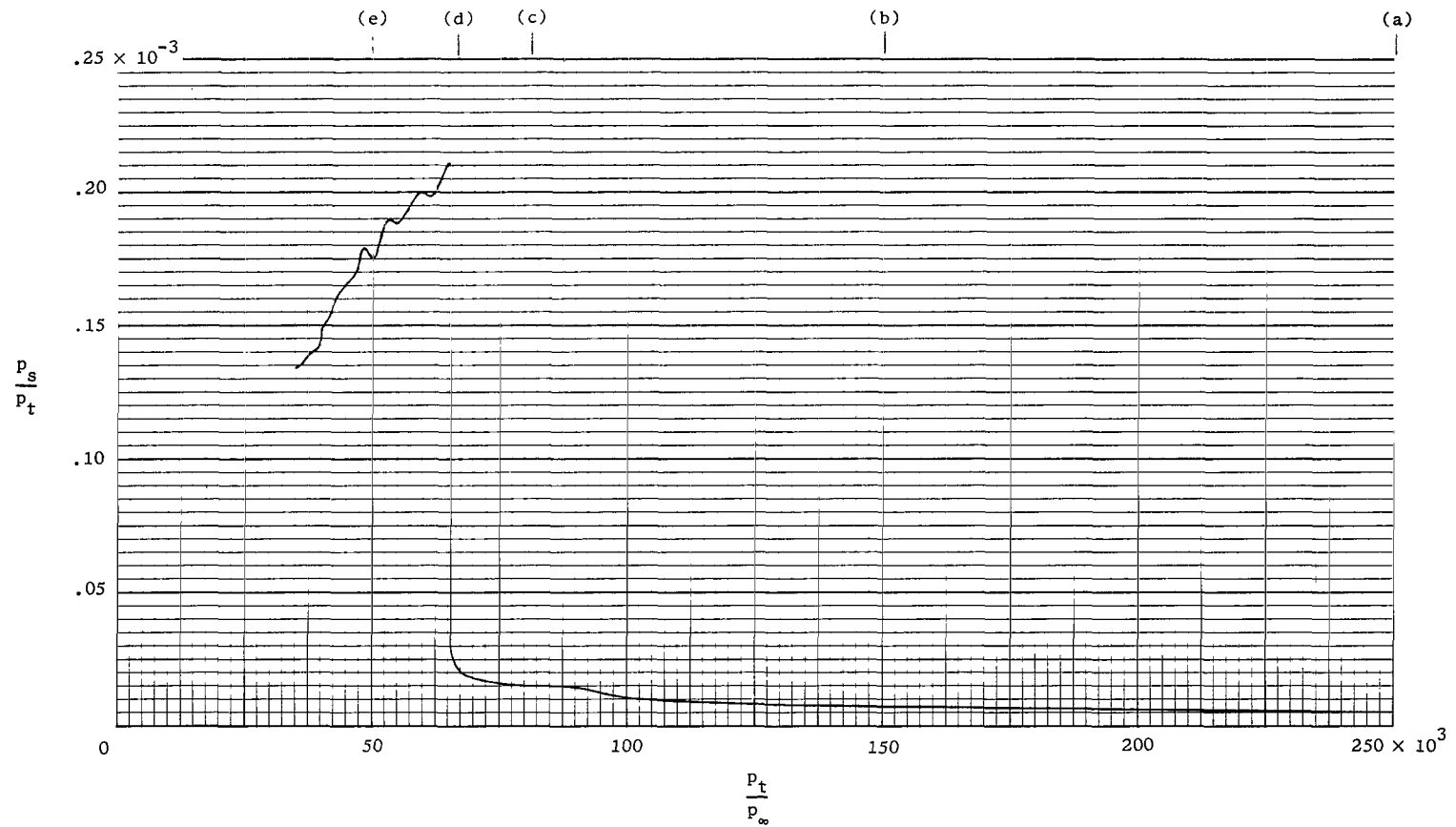
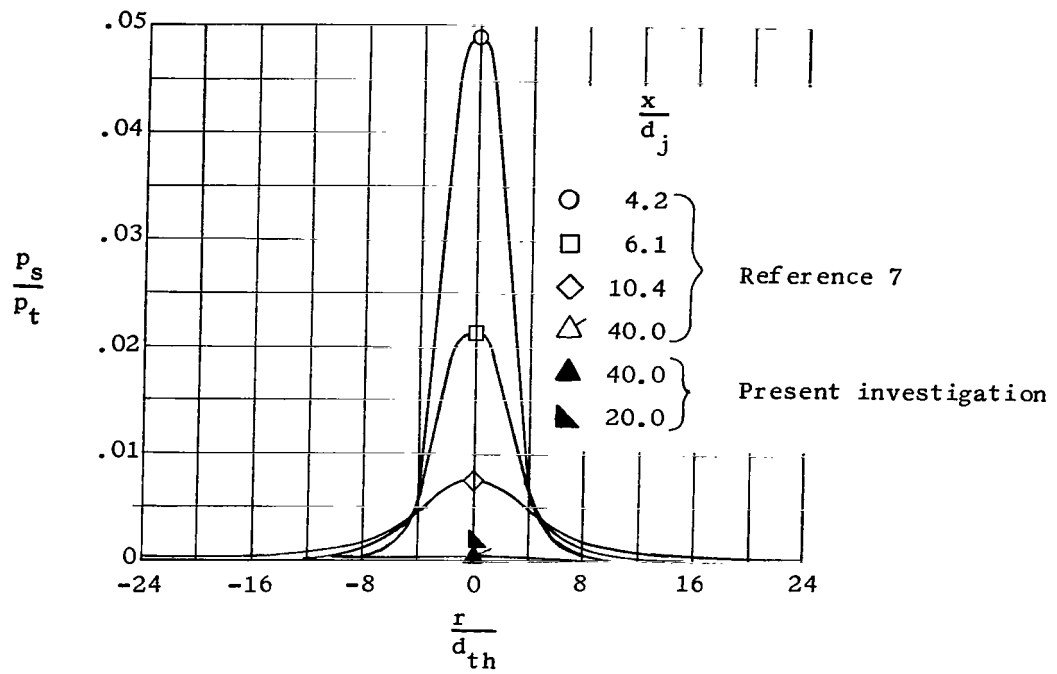
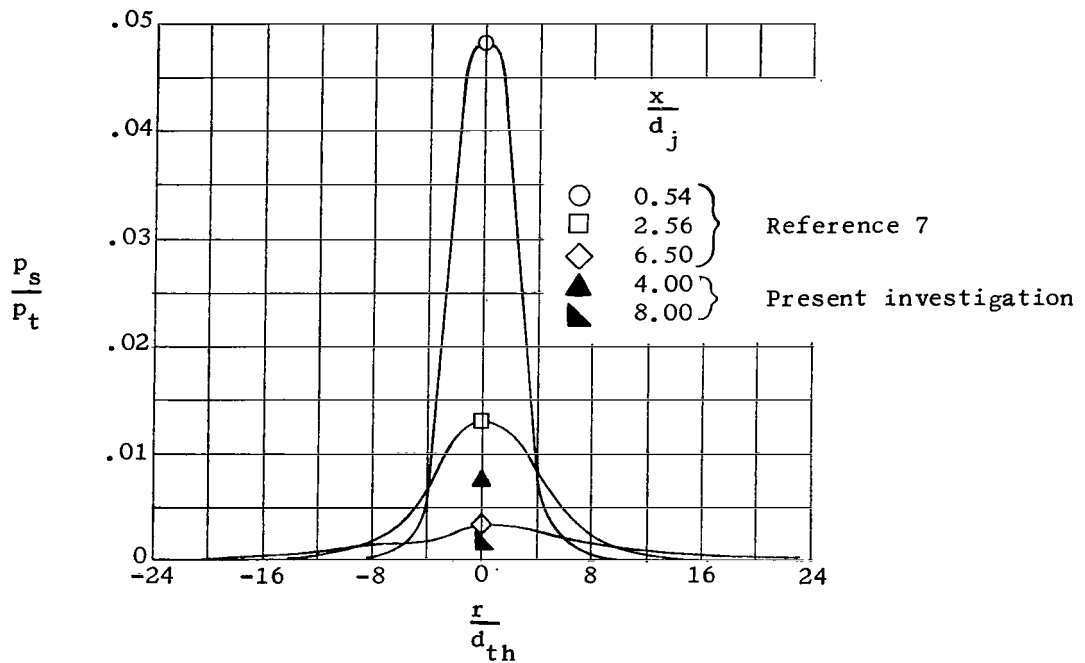


Figure 10.- Variation of impingement-surface center-point pressure distribution with ratio of nozzle total pressure to ambient pressure.
 $M_j = 5.0$; $x/d_j = 80$. Lower case letters identify sketches of figure 9.

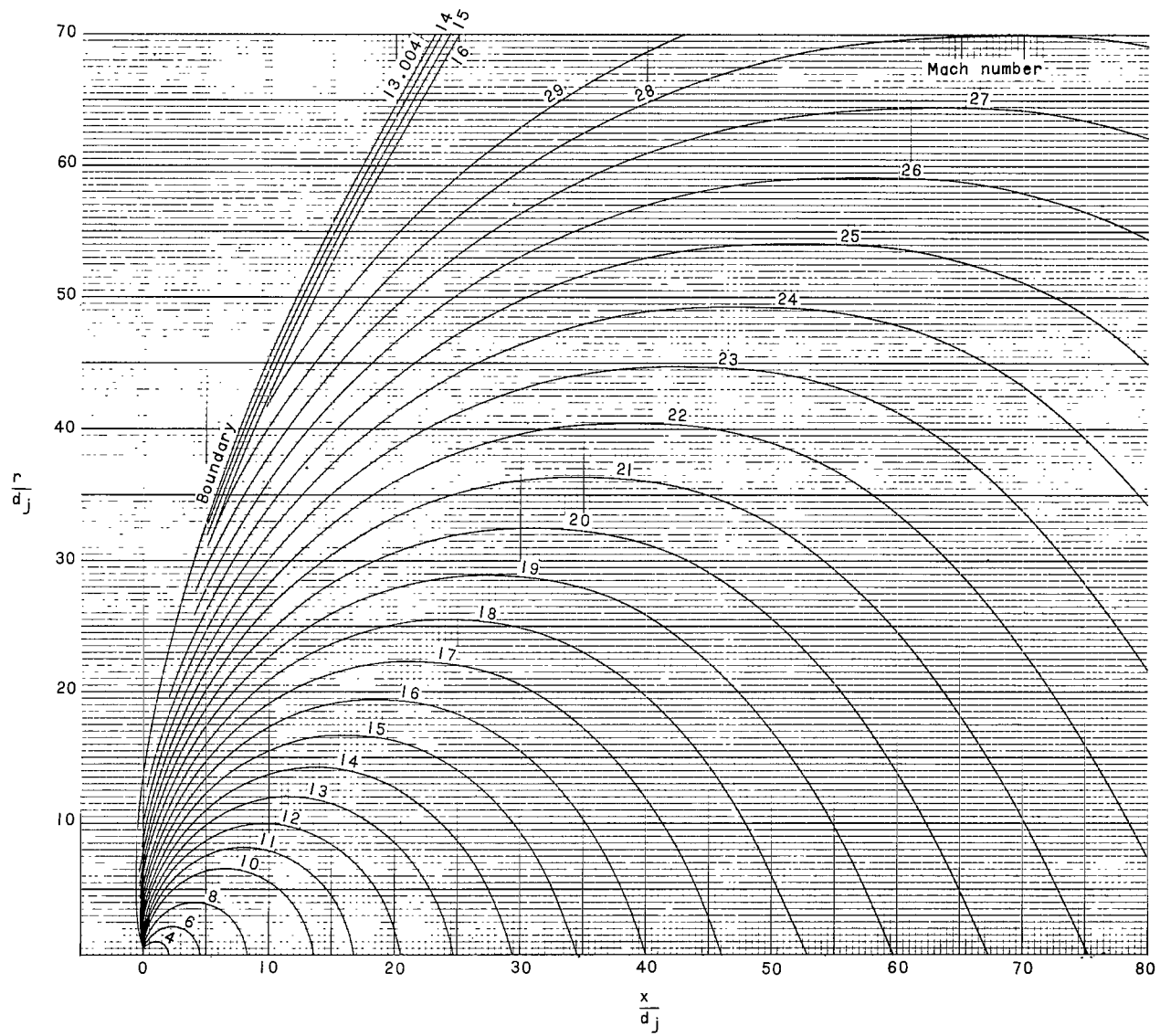


(a) $M_j = 1.0$.



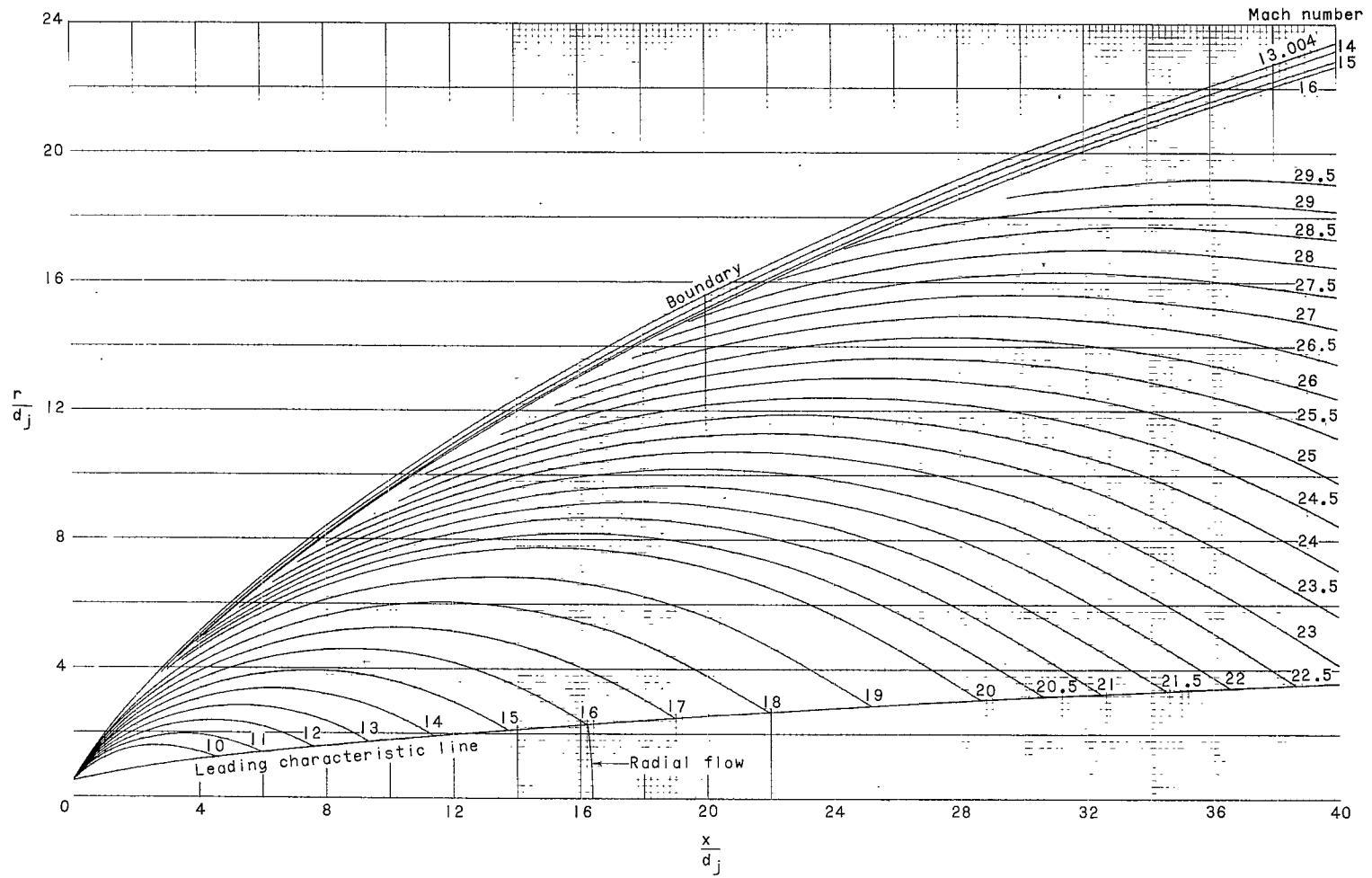
(b) $M_j = 5.0$; $\theta_n = 15^\circ$.

Figure 11.- Comparison of data from present investigation with data from reference 7. $p_t/p_\infty = 288 \times 10^3$.



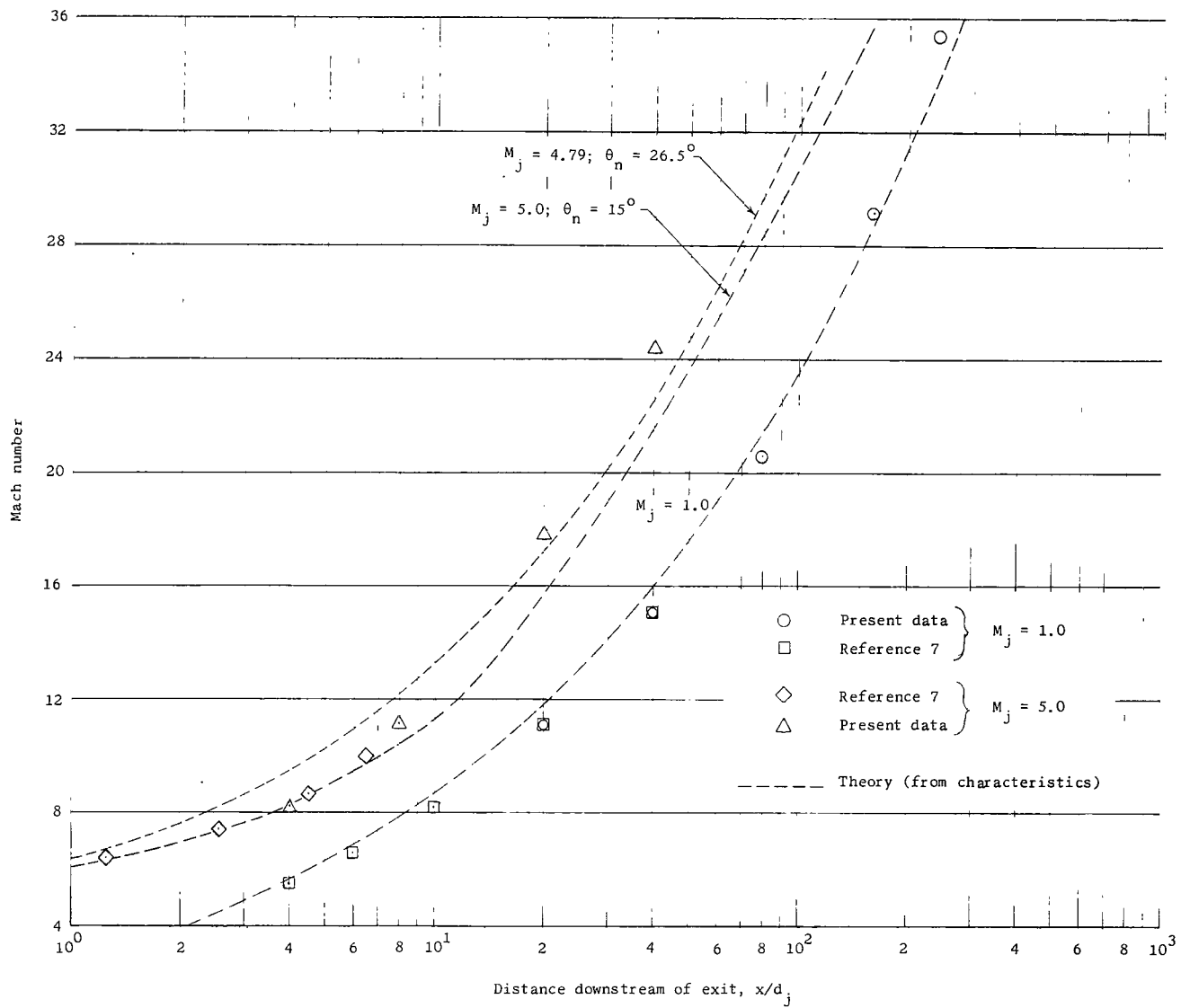
(a) $M_j = 1.0$.

Figure 12.- Theoretically calculated contour lines of constant Mach number within nozzle exhaust plume. $p_t/p_\infty = 250 \times 10^3$.



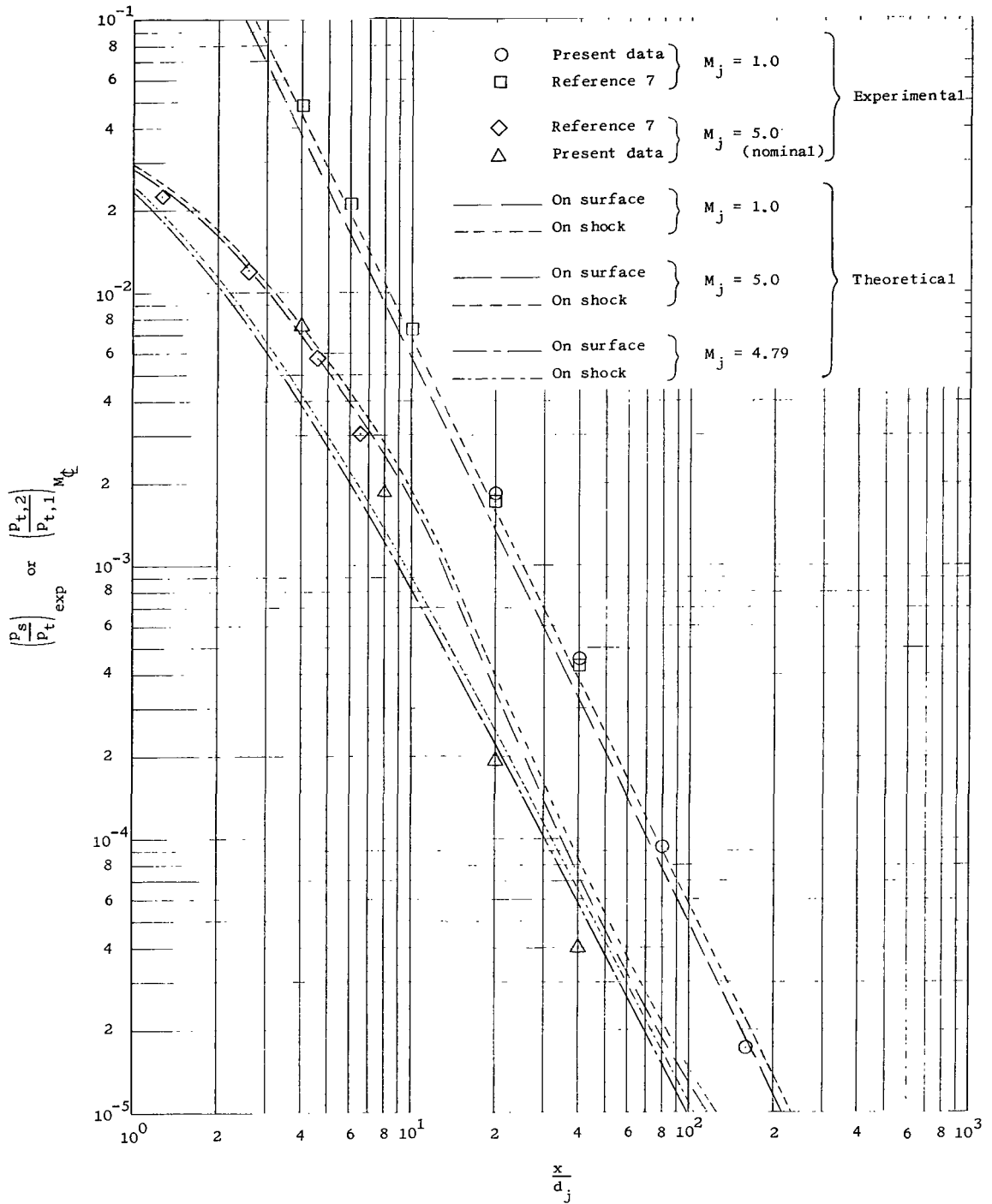
(b) $M_j = 4.79$; $\theta_n = 26.5^\circ$.

Figure 12- Concluded.



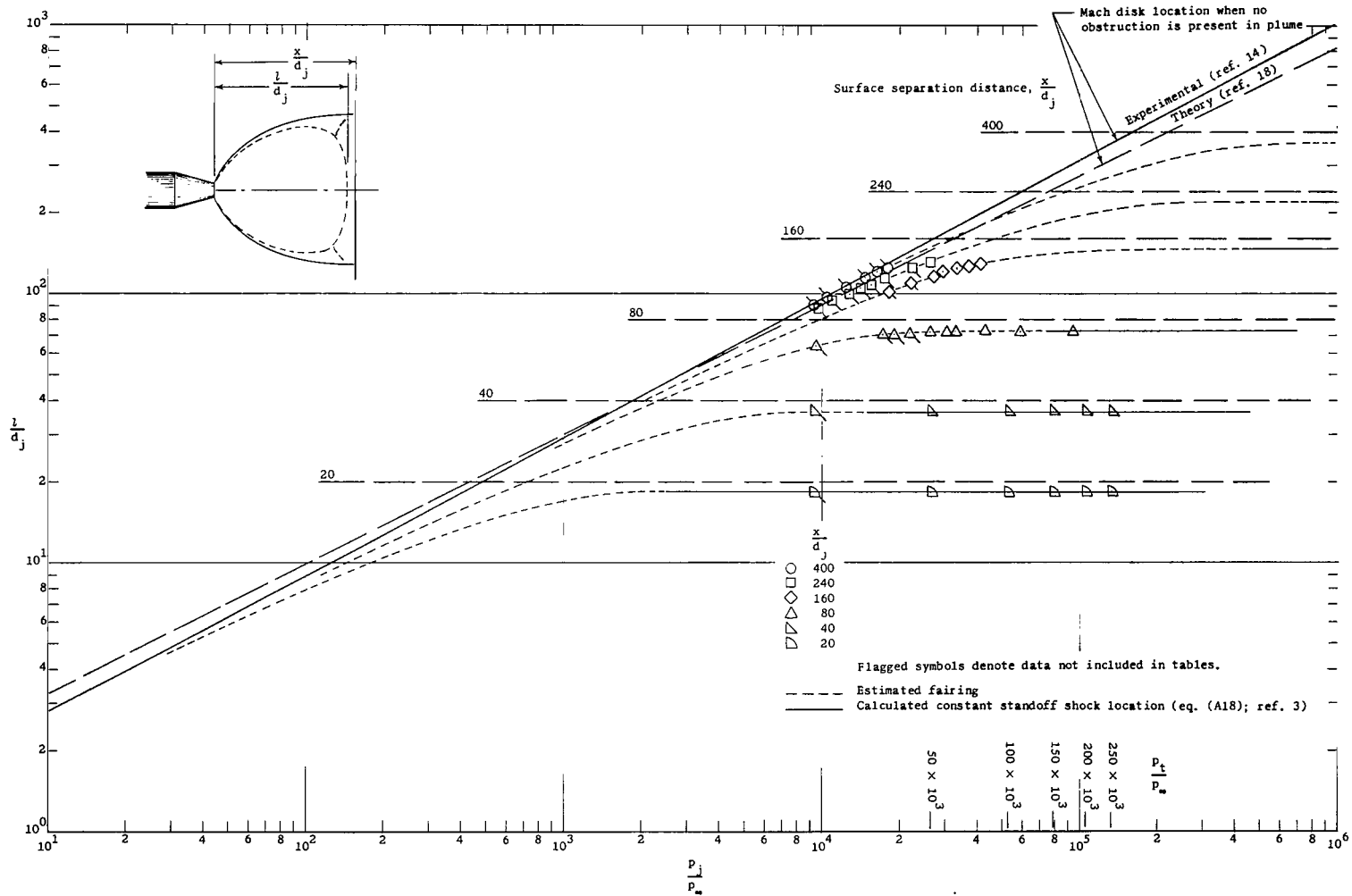
(a) Mach number distribution.

Figure 13.- Distribution of experimental and theoretical data along exhaust-plume axis. $p_t/p_\infty = 250 \times 10^3$. Experimental data plotted at actual surface location, x/d_j .



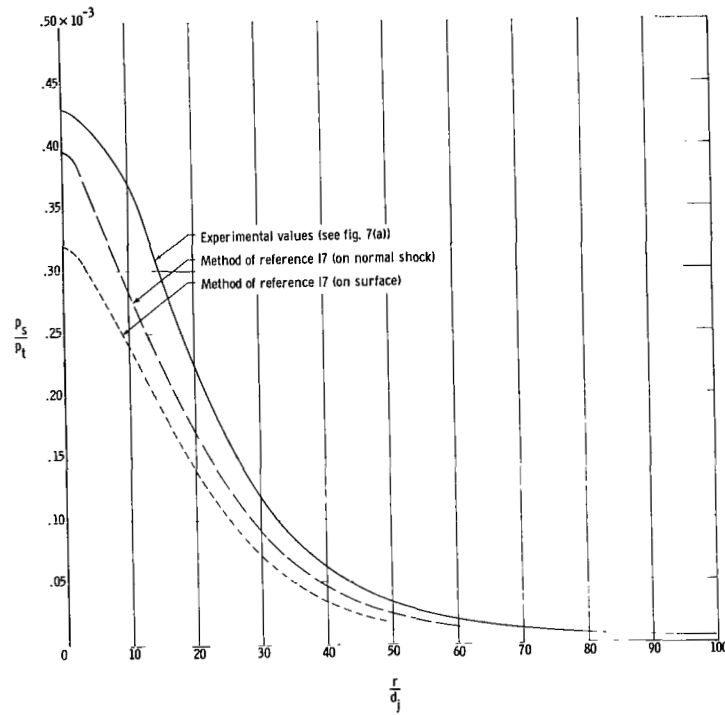
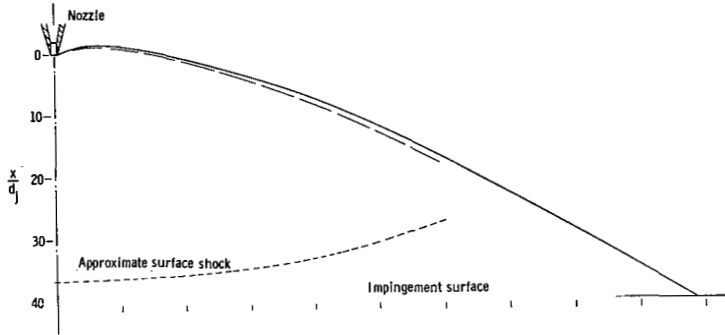
(b) Pressure behind a normal shock or surface center-point pressure.

Figure 13.- Concluded.

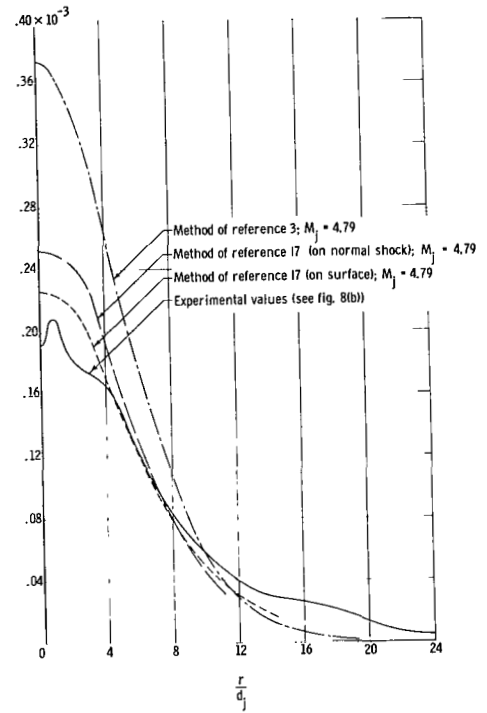
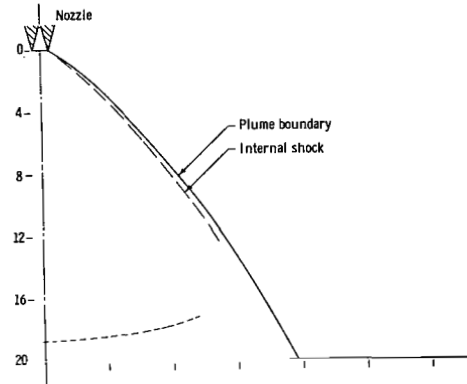


(a) $M_j = 1.0$.

Figure 14.- Effect of nozzle pressure ratio and nozzle-to-surface separation distance upon the shock position. x/d_j values have been measured from schlieren movies.



(a) $M_j = 1.0; \frac{X}{d_j} = 40.$



(b) $M_j = 5.0; \frac{X}{d_j} = 20.$

Figure 15.- Comparison of calculated and experimental pressure distributions on impingement surface. $p_t/p_\infty = 250 \times 10^3.$

"The aeronautical and space activities of the United States shall be conducted so as to contribute . . . to the expansion of human knowledge of phenomena in the atmosphere and space. The Administration shall provide for the widest practicable and appropriate dissemination of information concerning its activities and the results thereof."

—NATIONAL AERONAUTICS AND SPACE ACT OF 1958

NASA SCIENTIFIC AND TECHNICAL PUBLICATIONS

TECHNICAL REPORTS: Scientific and technical information considered important, complete, and a lasting contribution to existing knowledge.

TECHNICAL NOTES: Information less broad in scope but nevertheless of importance as a contribution to existing knowledge.

TECHNICAL MEMORANDUMS: Information receiving limited distribution because of preliminary data, security classification, or other reasons.

CONTRACTOR REPORTS: Technical information generated in connection with a NASA contract or grant and released under NASA auspices.

TECHNICAL TRANSLATIONS: Information published in a foreign language considered to merit NASA distribution in English.

TECHNICAL REPRINTS: Information derived from NASA activities and initially published in the form of journal articles.

SPECIAL PUBLICATIONS: Information derived from or of value to NASA activities but not necessarily reporting the results of individual NASA-programmed scientific efforts. Publications include conference proceedings, monographs, data compilations, handbooks, sourcebooks, and special bibliographies.

Details on the availability of these publications may be obtained from:

SCIENTIFIC AND TECHNICAL INFORMATION DIVISION
NATIONAL AERONAUTICS AND SPACE ADMINISTRATION

Washington, D.C. 20546